

# Time-Reversed Energy Sourced Through Localized Antennae

by

Gemstone Team TESLA

Submitted to the Department of Physics  
in partial fulfillment of the requirements for the degree of

Gemstone Honors Program

at the

UNIVERSITY OF MARYLAND, COLLEGE PARK

May 2016

© University of Maryland, College Park 2016. All rights reserved.

Author .....  
Department of Physics  
April 15, 2016

Certified by .....  
Steven Anlage  
Professor  
Thesis Supervisor

Accepted by .....  
Frank Coale  
Director, Gemstone Program



# Time-Reversed Energy Sourced Through Localized Antennae

by

Gemstone Team TESLA

Submitted to the Department of Physics  
on April 15, 2016, in partial fulfillment of the  
requirements for the degree of  
Gemstone Honors Program

## Abstract

We investigate the application of time reversed electromagnetic wave propagation to transmit energy to a moving target in a reverberant environment. “Time reversal” is a signal focusing method that exploits the time reversal invariance of the lossless wave equation to direct signals on a single point inside a complex scattering environment. In this work, we explore the properties of time-reversed microwave pulses in a low-loss ray chaotic chamber. We measure the spatial profile of the collapsing wavefront around the target antenna, and demonstrate that time reversal can be used to transfer energy to a receiver in motion. We discuss the results of these experiments, and explore their implications for a wireless power transmission system based on time reversal

Thesis Supervisor: Steven Anlage

Title: Professor



## Acknowledgments

Thank you mom.



# Contents

<b>1</b>	<b>Introduction</b>	<b>15</b>
<b>2</b>	<b>Literature Review</b>	<b>17</b>
2.1	Wireless Power Transfer Technologies . . . . .	17
2.1.1	Efficiency . . . . .	18
2.1.2	Range . . . . .	19
2.1.3	Maximum Power . . . . .	19
2.1.4	Active or Passive Transmission . . . . .	19
2.1.5	Size and Weight of Transmitting and Receiving Units . . . . .	19
2.1.6	Health Concerns . . . . .	20
2.2	Technologies . . . . .	20
2.2.1	Very Short Range . . . . .	20
2.2.2	Medium Range . . . . .	21
2.3	Long Range . . . . .	23
2.3.1	WiTricity . . . . .	26
2.4	Time Reversal . . . . .	27
2.4.1	Conceptual of Time Reversal . . . . .	27
2.4.2	History of Time Reversal Research . . . . .	28
2.5	Experimental Work . . . . .	32
<b>3</b>	<b>Methodology for Conducting Linear Time Reversal</b>	<b>33</b>
<b>4</b>	<b>Overlapping Reconstructions</b>	<b>37</b>

4.1	Purpose . . . . .	37
4.2	Methodology . . . . .	37
4.3	Results . . . . .	38
4.4	Discussion . . . . .	39
<b>5</b>	<b>Spatial Profiling</b>	<b>41</b>
<b>6</b>	<b>Moving Reconstructions</b>	<b>43</b>
<b>7</b>	<b>Methodology for Conducting Nonlinear Time Reversal</b>	<b>45</b>
<b>8</b>	<b>Using Nonlinear Time Reversal for Selective Reconstructions</b>	<b>47</b>
<b>9</b>	<b>Numerical Simulations of the Nonlinear Time Reversal Process</b>	<b>49</b>
9.1	Purpose . . . . .	49
9.2	Methodology . . . . .	50
9.2.1	Equipment . . . . .	50
9.2.2	Time-Reversal and Nonlinear Sona Extraction . . . . .	51
9.2.3	Defining and Controlling the Nonlinear Element . . . . .	53
9.3	Results . . . . .	55
9.3.1	Simultaneous Nonlinear Time Reversal . . . . .	55
9.3.2	Discussion of Simultaneous Nonlinear Reconstructions . . . . .	58
9.3.3	Simulation of Selective Collapse of NLTR . . . . .	59
9.3.4	Discussion of Selective Nonlinear Time Reversal . . . . .	63
9.3.5	Simulation of Transmission Efficiency of NLTR Process . . . . .	63
9.4	Conclusion . . . . .	65
<b>10</b>	<b>Nanorods</b>	<b>67</b>
<b>11</b>	<b>Rectification</b>	<b>69</b>
11.1	Goals of Rectenna . . . . .	69
11.2	Diode Selection and Testing . . . . .	70
11.3	Antenna Design . . . . .	71

11.4 Rectenna Testing . . . . .	73
11.4.1 DC Power Characterization . . . . .	73
11.4.2 Harmonic Generation . . . . .	76
11.5 Discussion . . . . .	78
<b>12 Conclusion</b>	<b>81</b>
12.1 Future Work . . . . .	81
12.2 Summary . . . . .	81
<b>A Appendix A</b>	<b>83</b>
<b>B Appendix B</b>	<b>85</b>



# List of Figures

2-1	TODO:I NEED A CAPTION	24
2-2	TODO:I NEED A CAPTION	24
2-3	TODO:I NEED A CAPTION	25
2-4	WiTricity schematic	27
3-1	Lab equipment setup	34
3-2	Conceptual overview of linear time reversal	35
4-1	Overlapping sonas	38
4-2	Overlapping reconstructions	39
4-3	Power from overlapping reconstructions	40
7-1	Conceptual overview of nonlinear time reversal	46
9-1	Example of inverted and non-inverted interrogation signals	52
9-2	Demonstration of pulse inversion	53
9-3	CST circuit model of a diode	54
9-4	I-V curves of diodes with different voltage knees	55
9-5	The Cut Box Model	57
9-6	$S_{11}$ spectrum of the Cut Box Model	57
9-7	Simultaneous reconstructions on two diodes	58
9-8	Nonlinear response due to different diode settings	60
9-9	Selective reconstruction on a $V_k^{low}$ diode	61
9-10	Selective reconstruction on a $V_k^{high}$ diode	62
9-11	Example transfer efficiency for a two-diode simultaneous reconstruction	64

9-12 The Room Model . . . . .	65
11-1 Rectenna design . . . . .	72
11-3 Rectified DC power . . . . .	75
11-5 Rectification efficiency . . . . .	78
11-6 Experimental setup for harmonic generation testing. . . . .	78

# List of Tables

2.1 Comparison of wireless technology companies and their products' capabilities . . . . .	18
9.1 Computer specifications . . . . .	51
11.1 Datasheet for diode used in rectenna construction . . . . .	71



# Chapter 1

## Introduction

In 1998, accessing the Internet required a clunky desktop computer and a dial-up subscription. When Apple integrated WiFi into its iBook computers under the brand name “AirPort” the following year, it forced other industry giants to compete and revolutionized wireless networking [2]. If not for the adoption of this technology along with the advent of wireless data-enabled and commercially available cell phones such as Nokia’s Communicator 9000 [1], cell phones would never have evolved to surpass their primary function as telephones and become the communication necessity they are today.

The ubiquity of WiFi and wireless communication revolutionized the way society interacts with the Internet. Suddenly, portable devices became powerful standalone devices rather than accessories to their desk-bound counterparts. Cell phones rivaled computers in necessity and ubiquity, and eclipsed their predecessors in terms of productivity. Coffee shops, airports, and hotels transformed from physical meeting places to universal hotspots, enabling the masses to bridge distances, connect instantly, and effectively trivialize time and space quite literally in the palms of their hands. This is the power of wireless technology.

So then, why does society continue to labor under the burden of wires? Having enjoyed rewards of another relatively nascent wireless technology, why do we hesitate to cut the cord?

Wireless power transfer (WPT)-enabled mobile devices have the potential to be a

disruptive technology on the consumer technology market. Investments in WPT have grown dramatically in the past decade, and more technologies have started integrating WPT into their systems at the consumer level.

The result is a growing number of WPT methods seeing practical application. These techniques can successfully power and charge a wide range of consumer products, from cell phones to cars. However, they still face significant disadvantages in transmission distance and efficiency. Most require line of sight to operate.

Gemstone Team TESLA proposes time-reversed electromagnetic wave propagation (to be abbreviated “time-reversal” or “TR” in this document) as a novel WPT method. In particular, TR’s ability to maintain connection even when line of sight is lost opens up a new range of possible applications. To support this proposal, the team has performed a number of exploratory experiments on the topic of TR applied to WPT. These experiments are concerned primarily with understanding the fundamental engineering realities that would be necessary to build a working TR WPT system.

In this thesis, TESLA overviews the state of the art of both consumer wireless power transfer technologies and time reversal. Major innovations are outlined, as are current limitations. The team’s experiments are then detailed individually. The purpose, methodology, and results for each experiment are explained. The results of each experiment and their significance are then discussed in the context of TR WPT. The results of the team as a whole are discussed in a similar way. Finally, the team makes suggestions for future research that could be made in this field, for the benefit of future researchers.

# Chapter 2

## Literature Review

Commercial wireless power transfer technologies have developed as a response to both the ubiquity of mobile devices and limitations in traditional wired power. These technologies differ in range, efficacy, and method, but suggest an overall attempt to shift away from traditional charging mechanisms. This literature review will focus on the distinct methods that make up the current state-of-the-art of wireless power. These methods and companies are not meant to be exhaustive, but should be recognized as a birdâŽs-eye-view toward these liminal technologies. TODO:*Is the previous sentence too long-winded?* This review will additionally explore WPT technologies based on their applicable ranges.

At the conclusion of this state-of-the-art overview, we will discuss both the general operation of time reversal and the historical developments of the TR field. This will include the acoustical roots of TR by Claire Prada and Matthias Fink, later communication accomplishments by Steven Anlage, and TESLAâŽs modern WPT application. TODO:*Too flashy? Maybe remove*

### 2.1 Wireless Power Transfer Technologies

Several groups have already made practical WPT technologies. In this paper Powermat, WiTricity, Wattup, uBeam, Cota, and Wicharge will be considered as the state of the art WPT methods. These technologies will be compared using several different

Company	Method of Power Transfer	Max Power Delivered (W)TODO:cite	Approx. Range (ft.)
Cota	Concentrated Microwaves	1	30
Powermat	Inductive Coupling	5 to 50	Touching
uBeam	Ultrasound	Unknown (minimum 1.5)	3 to 13
WattUp	RF	10	15
Wi-Charge	Laser	10	30
WiTricity	Inductive Coupling	Scalable, on the order of 1000	7

Table 2.1: Comparison chart of wireless technology companies and their products' capabilities<sup>1</sup>

metrics, defined here. The capabilities of these technologies under these metrics are summarized in Table 2.1, and discussed in detail. TODO:*Why are we considering these in detail?*

As can be seen, the different WPT technologies vary wildly in both their methods of operation and their intended application. Comparing different WPT technologies is difficult because the measures of characterizing performance used in Table 2.1 are poorly defined. Metrics for operation are defined separately by individual companies, when they are defined at all. The desire by companies to protect their IP encourages this confusion. We will specify our own definitions of performance metrics important to this paper.TODO:*clean this up a bit*

### 2.1.1 Efficiency

Efficiency in particular is difficult to quantify, as there does not currently exist a standardized definition used by all parties. In the literature, efficiency of transfer has

---

<sup>1</sup>Some companies are still in their early stages and thus have not released full details about their technology yet. The information in this table reflects all known publicly disclosed information at the time of writing.

included: the amount of power drawn by the transmitter compared by the amount of energy delivered to the target. the transfer between antennas within a setup, with other losses (such as those due to rectifiers after transmission) being ignored.

Here, the team will define efficiency as TODO:**BLANKITY BLANKITY BLANK.**

### **2.1.2 Range**

Range is defined here as the maximum distance that a given amount of power can be transmitted.

TODO:NEED TO ADD A TABLE HERE OF WHAT THE RANGES ARE: <5ft, <15ft, <30? s

### **2.1.3 Maximum Power**

The maximum amount of power that can be transmitted to a target using a given technology.

Maximum power limits the devices that can be powered by a given technology. While high power transmission is not important for all devices, a larger range of power improves the flexibility of the technology.

### **2.1.4 Active or Passive Transmission**

One characterization of WPT technologies can be made from considering whether or not the receiver requires power. WPT technologies that require power to complete the process can be described as an active transmission system. A passive technique is one in which the receiver does not require power.

### **2.1.5 Size and Weight of Transmitting and Receiving Units**

With the use of WPT technologies, the viability of the technologies towards particular applications needs to be examined. Some example criteria for examining this viability are size and weight constraints of the application. These criteria are emphasized in

the application of WPT for mobile devices, where WPT technologies with smaller and lighter receivers are better suited.

### 2.1.6 Health Concerns

TODO:ScottâŽs Colloquium discussion

## 2.2 Technologies

TODO:NOTE: NEED TO MAKE SURE THAT TONE RE: OTHER COMPANIES IS OBJECTIVE.

TODO:WE NEED AN INTRO TO THIS

TODO:We need a delineation of the ranges

### 2.2.1 Very Short Range

#### Powermat

The most restrictive technology in terms of range is that of Powermat. Devices are charged by being placed on the charging mat. Harnessing inductive coupling, the same method used to charge electric toothbrushes, Powermat has virtually no charging range, as the device and the charger must be in full contact. The technology is capable of charging multiple devices, and it has created compatibility devices for those devices which are not sold pre-Powermat-enabled.

As the charging mat is wired, its range is still restricted to the length of a power cord. What Powermat saves is the burden of two to three more wires and the motion of plugging the charging cord into a device—if that. If the device is not compliant with the Powermat standard, then it must be plugged into a compatibility device anyway. The mat can deliver between 5 and 50W, making it a very effective charging tool, but it reaps virtually none of the potential benefits of wireless charging.

## 2.2.2 Medium Range

### WiTricity

### WattUp

Our next mid-range WPT company is named WattUp. The central idea of this company's method is to use bluetooth to transfer RF signals about the receiver's location relative to the transmitter so that the transmitter may focus energy on the receiver. Once it has locked in a signal, it may boost the output power from mW RF signals to multiple W RF signals such that the receiver can charge. WattUp highlights two main features to its technology: (1) the range over which 1–4 W may be quickly and safely transmitted and (2) the relatively large number of devices that may be powered at once (currently 12, with 24 being available in the future).

As is the case with the other investigated WPT companies, the primary feasibility concern is the range and power that the technology offers. WattUp cites that they may deliver up to 4W to a 4 devices simultaneously within 0-5 feet of the transmitter, 2W to 4 devices simultaneously within 5–10 feet, and 1 W within 10–15 feet. This linear decrease in power with increasing range is similar to the trend seen with WiTricity, as previously discussed. These numbers only represent the current model and demonstration version of the technology. WattUp boasts that for ranges <5 feet, the device will charge as if it were plugged into a wall outlet, for 5-10 feet, the device will resemble USB port charging from a computer, and for 10–15 feet users can still slower charge rates, Based on the aforementioned values provided by WattUp, the overall max range is ~15 feet with a max output power of ~10 W, although these two conditions may not be met at the same time.

The technology itself uses two separate RF frequencies to perform wireless charging, representing both the Bluetooth communication (2.4 GHz) and power transfer frequency (5.7 GHz). Both of these frequencies are allowed unlicensed frequency bands that are known to be used for wireless communication. We believe that WattUp chose to use separate frequencies in order to more easily differentiate the signals used for either targeting or power transfer. As the targeting algorithm is proprietary,

we are unable to comment on their exact methodology for targeting the receiver.

In terms of feasibility for commercialization, the transmitter is simply a 12-in x 12-in antenna array, resembling an oversized router. The receiver is much smaller, being only 1.5-in x 1.5-in that may easily be either embedded in a device or made into a small case or add-on to the device. Given the small size of the transmitter and receiver, the technology is still able to lock onto a device within a matter of seconds. The technology has been deemed safe by the FCC, and WattUp states that “based on our preliminary calculations, the SAR at our receiver should be well below that of a typical cellular signal”. The combination of these two aspects coupled with the notable range, transmittable power, and allowed number of devices to charge causes WattUp to be a very viable commercial technology for the future. The major setback with this technology is that it requires a constant feedback loop of information from the Bluetooth connection. This implies that if a device is powered off, then it may not receive any power. Our process of NLTR would circumvent this problem; whereby, a the nonlinear element inside the device would allow WPT to occur even in a device has a power level of 0%.

## **uBeam**

The other primary medium range WPT titled uBeam uses an entirely unique method compared to other companies/methods, relying on ultrasonic waves rather than electromagnetic waves. One can imagine their system as an extremely high power microphone and speaker combination that specifically sends the sound to a device location. Although uBeam is unique in its approach, it boasts comparable range and power levels when discussed next to other WPT companies.

The first difficulty to using sound waves as opposed to electromagnetic waves is the inherent dissipative nature of air as a medium. Due to this characteristic, uBeam uses output sound levels of 145–155 dB ( $316 - 3000 \frac{W}{m^2}$ ), comparable to the sound produced by a jet engine or shotgun blast. In order for this level of sound to be used safely, uBeam a transmission frequencies of 45–75 kHz, as this is far above the audible range of both humans and animals. As an extra safety measure, uBeam cites that “if

a person were to be exposed to the uBeam ultrasound source, 99.9% of the emitted ultrasound will bounce off the skin”. These considerations have allowed uBeam to stay well within the FDA safety regulations. uBeam uses a phased array transmitter with thousands of antennas that result in a power range of 1–4 m. Although the tracking and targeting algorithm is proprietary in nature, uBeam boasts the ability to maintain power transfer while the receiver is moving, although uBeam does not cite specific speeds. One significant drawback to uBeam is that it requires line of sight in order to work due to the nature of sound as a mechanical oscillation. For example, if a cell phone is in a user’s pocket, then it will not be able to be powered as the user’s clothing will block or extremely dampen the ultrasonic waves.

The main benefits that uBeam possesses include its moderate range, quick lock on time, and ability to power moving devices. Still, the main problem that uBeam does not cite is the overall efficiency of the power transfer. Using 145–155 dB is an extremely high power output from the transmitter. A reasonable output at the receiver is on the order of 1–10 s of watts. This disparity raises doubts that uBeam could be feasible WPT technology given the power input needed to produce such high dB levels is on the order of hundreds of watts. Using NLTR as a method of WPT possesses all the benefits of uBeam without the potentially small transfer efficiency.

## 2.3 Long Range

Two technologies drastically exceed their counterparts in range: Cota and Wi-Charge.

### Cota

Cota uses concentrated microwaves to create “pockets of energy” at precise locations. The power-seeking device sends out pulses regularly, which, when picked up by a Cota system, trigger the system to send out a high energy pulse targeted specifically to the device’s location.

The Cota system consists of two parts: a charger and a receiver. The Cota receivers built into devices and batteries regularly send out omnidirectional beacon

signals. Once the Cota charger receives these beacons, it returns thousands of targeted signals that build hotspots of energy at only the precise locations of the beacons' origins. The charger uses 20,000 antennas to determine the exact direction the signal came from. This pinpoint precision targeting of energy safely and efficiently powers all Cota-equipped devices and batteries within its effective radius, even as they move around the room.

The technology has achieved a 30 ft range and a max power delivery of about 1W, offering a comfortable operating radius and charging speed at about one-third the charging time via regular USB cable. It also cites the capability to charge as many devices as desired. However, it uses Bluetooth to link the charger to the receiver(s), which is an overhead that encumbers the simplicity and speed of microwave concentration. Furthermore, utilizing the Bluetooth protocol requires that the power-seeking device constantly pulse, requesting power. This means that charging the device is contingent on the device already having enough power to send that request.

## Wi-Charge



Figure 2-1: TODO:I NEED A CAPTION



Figure 2-2: TODO:I NEED A CAPTION



Figure 2-3: TODO:I NEED A CAPTION

Also capable of a 30 ft operating radius, Wi-Charge uses lasers to create robust power transfer systems. To understand the system, it is necessary to discuss how a laser works. Consider Figure 2-1, which depicts two mirrors and an amplifier between them. Simply put, one photon, an energetic light particle, enters the amplifier and two come out. When the photons hit the mirror, they bounce back through amplifier in the opposite direction and two photons become four. This process repeats with each ricochet against a mirror, and the energy amplifies within the system. This process of recirculating light in a positive feedback loop with an amplifier creates a resonator.

When that resonator has one mirror that is very slightly transparent, as in Figure 2-1, then a focused, high powered beam is generated. This beam is a laser.

Any particles that do not travel along the axis between the two mirrors will hit the mirror at an odd angle and bounce out of the resonator. This is why only the photons that are traveling in the direction of the axis between the two mirrors will continue to amplify.

Wi-Charge took this traditional definition of a laser, and made a few clever modifications to better suit their purposes, shown in Figure 2-2.

First, they kept the components—two mirrors with an amplifier between them—but modified their arrangement. Second, they made the mirrors retro-reflectors which, unlike regular mirrors, reflect light back to their sources. The result is that the two mirrors spontaneously form a resonator when placed within each other's line of sight, and that the resonator is stalled immediately when the line of sight is broken.

Thus, if one the mirrors is attached to the device and the other is attached to the transmitter, then an inherent, yet safe amplification system is created. Thus, the first mirror and the amplifier are grouped together as the transmitter, and the second mirror and a photovoltaic cell are grouped together as the receiver. This is shown in Figure 2-3.

Wi-Charge is a long range wireless power solution that can deliver up to 10W of power [?]. It can latch onto targets almost instantaneously and cease beaming equally quickly, intrinsically. It can also power multiple devices. However, the feature that enables all of its strongest points is also its seemingly irreparable flaw: line-of-sight. While this system may work beautifully in a sparsely populated environment, in any thriving business or locale, such as the busy coffee shop or airport in which Wi-Charge envisions its products, there will be too many obstructions disrupting its line of sight. Thus, this fatal flaw renders Wi-Charge an impractical solution to the problem of WPT.

TODO:cite ?? above: <http://www.businesswire.com/news/home/20150310006473/en/Wi-Charge-Ushers-Era-Wireless-Device-Charging>

### 2.3.1 WiTricity

Boston-based company WiTricity® has expanded traditional magnetic induction using a method they call highly resonant magnetic coupling (HRMC). Whereas traditional magnetic induction operates at the range of centimeters, HRMC is applicable on the scale of meters. WiTricity® reports 50% efficiency at two meters, followed by 10% efficiency at four meters [15, 28]. HRMC have charged multiple devices without seemingly sacrificing overall efficiency [15]. The public demonstrations by WiTricity® show that HRMC can transmit power ranging from milliwatts to kilowatts, significantly more than was practical with traditional induction [15].

HRMC uses magnetic induction to transmit energy between two coupled antennas. HRMC continually adjusts the coupling of transmitter and receiver antennas to keep both at a mutual resonant frequency. This technique, impedance matching, minimizes the amount of wave reflection inside the transmitter and receiver circuits,

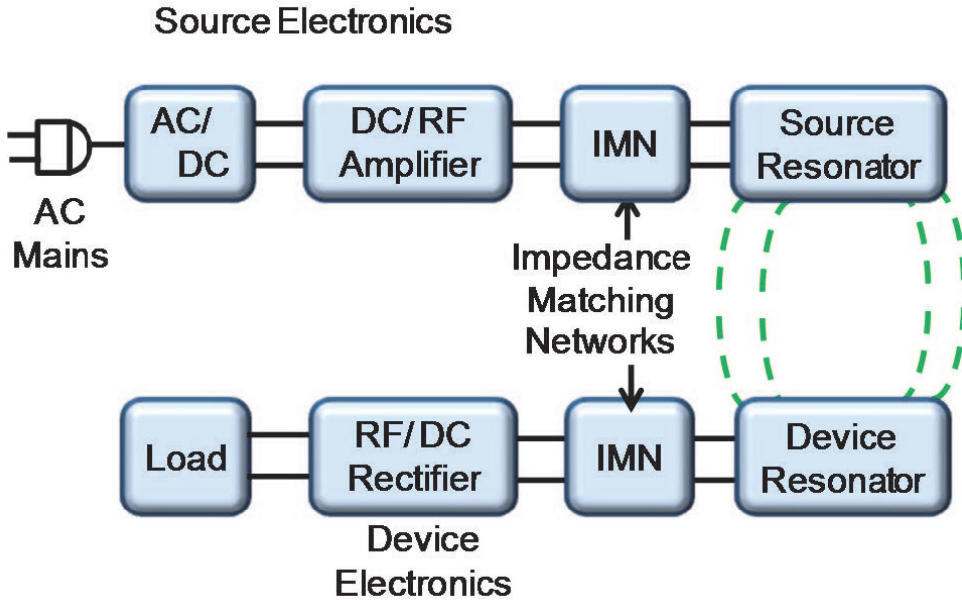


Figure 2-4: Schematic of WiTricity’s HRMC System [15]

maximizing the energy passed to the load component. This process requires a constant proprietary feedback mechanism to optimize the receiver for the given distance from the transmitter.

WiTricity has demonstrated that the range of HRMC can be increased through the use of coupled relays. These relays can be coupled with the transmitter, allowing the effective range of the transmitter to increase with minimal additional loss [5].

## 2.4 Time Reversal

### 2.4.1 Conceptual of Time Reversal

The lossless wave equation is time-reversal invariant: for any normally propagating wave taken to be a time-forward solution, there is a corresponding time-reversed solution representing that wave traveling in the opposite direction. The technique known as time reversal (TR) exploits this property of waves focus a signal onto the point of origin of another previous signal. TR can locate objects without prior knowledge of their position or their surrounding geometry.

A system that performs TR is called a time reversal mirror (TRM), sometimes simply shortened to mirror. A TRM consists of one or more transmitters to introduce waves into a chamber and one or more receivers to record the echoes from it. The transmitters and receivers may (but do not have to be) the same device. TR is most effective in echoic chambers that allow waves to reflect off of its interior geometry and return to the transmitters. Here we refer to such a chamber as “reverberant”.

TODO:[figure of gaussian and sona](#)

A TRM works by broadcasting a waveform into the reverberant chamber and recording the resultant echo. This echo will consist of many time-shifted overlays of the original waveform. This echo will be called a “sona” in this thesis. The sona is time reversed and rebroadcast, which will cause the waves to trace their paths in reverse and return to their source in a semi-coherent “reconstruction” of the original broadcast. Since it involves waves from many scattered paths all suddenly arriving at the same point, this phenomenon is also known as “collapse”.

TR is relatively versatile. If the technique is iterated exactly as described, the broadcasts will collapse more and more exactly on the strongest scatterer in the chamber [?]. Many other methods can be used to select targets more discriminately, and the generic TRM itself can be modified as well - for example, by recording directly from a target position, it is possible to create a secure channel between that point and the transmitter [8].

#### 2.4.2 History of Time Reversal Research

Team TESLA’s project hopes to overcome some of these limitations through a novel method: the use of electromagnetic time reversal (TR). TR is a proven technique in signal processing, with applications in acoustics as well as electromagnetics. Though its publicity is limited, there is a wealth of available literature regarding TR in certain specialized areas. Here we briefly describe the development and historical applications of the technique to illustrate where TESLA’s project will expand this literature.

Time reversal as a technique was first developed in the 1990s. Some of the earliest

and most influential work was conducted through teams led by Mathias Fink and Claire Prada of the University of Paris. These researchers used the technique to focus sound waves on “scatterers”, objects that reflect the pulses [19]. An array of transducers would fire a sonic pulse into some propagation medium and listen for the echo. The recording of that echo was reversed in the time domain and transmitted back into the medium. They repeated (iterated) this process, causing the acoustic signature of the strongest scatterer to appear more prominently each time. In this way, the team was able to iteratively focus on the scatterers without needing prior knowledge of their location. Prada and her team submitted this DORT (French acronym, English: Decomposition of the Time Reversal Operator) method as a process for finding cracks or faults in structural members [19]. More importantly, Prada et al. went on to demonstrate that the method could always resolve the brightest scatterer if given enough iterations, that it worked better in a heterogeneous medium than a homogenous one, and that it was both experimentally and mathematically possible to resolve multiple targets at once [20]. These discoveries generated significant interest in a subset of the acoustics research community.

Others in the field of acoustics went on to refine the DORT method as an imaging technique, and as the field gathered attention, further explored formalizing the problem in general. An excellent example of the latter is the theoretical work by D. H. Chamber in his 2007 examination of TR for target detection and characterization [6]. In 2010, Nguyen and Gan developed a way to extract much more information from an anisotropic (directionally distinct) scatterer, including its rough shape, density, and radius. In doing so, they developed a faster mathematical approach to locating their scatterers that relied on several good approximations instead of one exhaustive computation [18]. Also in 2010, Barbieri and Meo made a large contribution to the field by bringing together the DORT method, which works in linear environments, and another similar method for working in nonlinear environments. This allowed them to resolve and distinguish between linear scatterers such as holes and nonlinear scatterers such as cracks [4].

Imaging is not the only application for a focusing method, however, and others

adapted the existing body of TR research to new problems. The reciprocity of the wave function that Fink and Prada relied on to develop the technique holds for all waves it can be used to model—this means that the time reversal operation works much the same way with electromagnetic waves as it does with sound waves [6]. This was explored as early as 1999, but was largely concerned with the same imaging problems occupying those in acoustics until at least 2007 [6]. However, that gradually began to change. In 2011, a team including graduate students from the University of Maryland posited that time reversal was an ideal mechanism for wireless communication [?]. In the same way that a sound wave could be made to collapse on a scatterer, they showed that an information packet could be made to collapse on a receiver. The team submitted this as a “green” or eco-friendly communication method, because information transfer could be accomplished using less energy [?]. Later, this same property was examined for its security benefits instead of its environmental ones. In February of 2013, a team of researchers at the University of Maryland, including Matthew Frazier and Steven Anlage, published a study discussing TR as a method to selectively send information in a chaotic wave environment [8] [25]. Essentially, the team was able to create an exclusive communication link to a certain object, without needing to know its location, and without interfering with nearby objects. In their experiment, they were able to transmit data (in the form of images) exclusively to a desired port, while the other port received only nonsense.

Beyond its practical applications, in the process, Frazier and his team used nonlinear elements to extend TR in new and exciting ways. Recall that in traditional TR many iterations are required to pinpoint the target. The addition of a significantly nonlinear element greatly simplifies the pinpointing process. When a wave strikes the element, harmonic frequencies are produced at integer multiples of the original frequency. These harmonics can be quickly located in the echoâŽs frequency domain and filtered to select them exclusively. The important distinction is that since the harmonics originated directly from the target antenna, all subsequent broadcasts of the TR signal will collapse on the antenna without the need for iteration [8]. Frazier and the others put forth several exciting directions to pursue with this concept: the

aforementioned secure communication channels, hyperthermic treatment of tumors, and a long range WPT system that eschews traditional high power beams. It is this last area that TESLA intends to explore.

## 2.5 Experimental Work

The following sections detail the research that TESLA has done in the field of TR WPT. These experiments are meant to accomplish several goals:

- Characterize the behaviors of TR relevant to WPT applications
- Understand fundamental limitations of TR applied to WPT
- Create a baseline for which future work can be done

The general methodology for the experiments is described. Then, the purpose, methodology, and results of individual experiments are discussed individually.

# Chapter 3

## Methodology for Conducting Linear Time Reversal

The majority of our experiments take place within an enclosed, reflective cavity called the Gigabox: an aluminum box with a metallic foil scattering paddle to make the ray trajectories more ergodic. Ray chaos ensures that a propagating pulse will eventually reach every point in the environment, which insures that many transmission channels are simultaneously excited, and this improves reconstruction fidelity. Up to five monopole antennas inject and extract electromagnetic signals from different ports in the enclosure depending on the experiment.

Our TRM consists of three pieces of microwave processing equipment and a desktop workstation. Interrogation pulses and time-reversed sona signals are created and broadcast using a Tektronix AWG7052 arbitrary waveform generator feeding an Agilent E8267D Vector PSG microwave source. A digital storage oscilloscope (DSO, Agilent DS091304A) is used to record waveforms of interest. MATLAB is used for signal processing and instrument control and coordination.

In many experiments, it is necessary to be able to “read” and “write” signals from the same port. Manually switching coaxial cables from the PSG to the DSO is slow and can destroy reconstructions, so we use four HP 8762C coaxial switches to reroute signals as required.

This hardware is laid out in Figure 3-1.

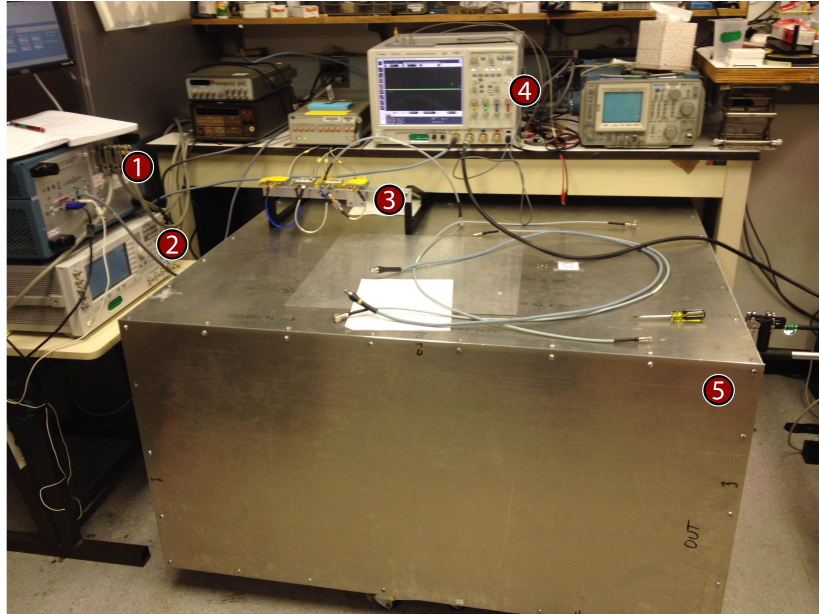


Figure 3-1: Lab equipment setup: 1) Tektronix AWG7052 Arbitrary Waveform Generator, 2) Agilent E8267D Vector PSG Microwave Source, 3) Array of four Hewlett-Packard 8762C coaxial switches, 4) Agilent DS091304A Digital Storage Oscilloscope, 5)  $1.06\ m^3$  aluminum “Gigabox” with interior conductive scattering paddle.

Our TR experiments fall into two main categories, which we refer to as linear and nonlinear. Nonlinear TR (or NLTR) makes use of harmonic reflections from the target to isolate it via Fourier transform after the sona is collected, a process similar to how we would envision a TR based WPT system to work. Linear TR or LTR refers to any experiment that locates the target another way, which in our case usually means taking a sona directly from the target’s location. It is experimentally much easier to get clean, strong reconstructions with LTR than with NLTR, so we use it for experiments investigating the behavior of the waves rather than the behavior of the target.

This section concerns LTR experiments. Conceptually, our general process for LTR in the Gigabox is as follows: we broadcast a Gaussian pulse from one port serving as a transmitter and collect a sona from another serving as a receiver. That sona is time reversed and rebroadcast from the transmitting port, which will cause a slightly distorted version of the original Gaussian pulse to reconstruct at the receiver. This process is illustrated in Figure 3-2.

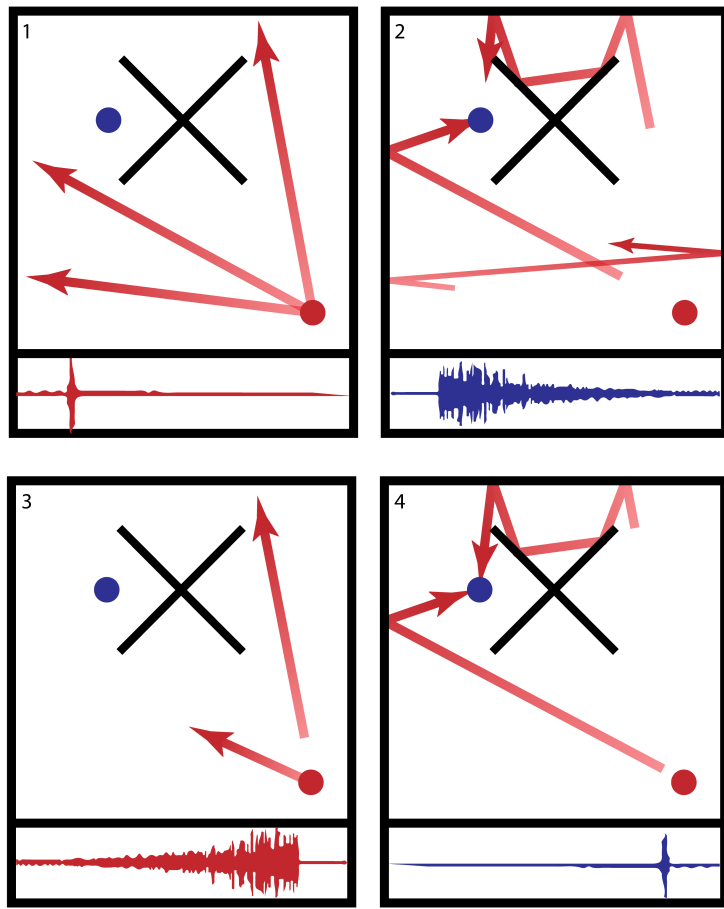


Figure 3-2: Reading order from top left: 1) The TRM broadcasts a signal (in this case, a pulse, pictured in the inset below the panel) into the cavity, which 2) reverberates within the cavity. Some of the reflections incoherently reach the receiver as the sona, represented in blue in the inset. 3) The TRM time reverses the sona, then re-emits it into the cavity. 4) The time reversed waves coherently collapse back on the receiver in a slightly distorted reconstruction of the original pulse (inset, blue).

TODO: OUGHT TO HAVE AN OUTRO HERE



# Chapter 4

## Overlapping Reconstructions

### 4.1 Purpose

Frazier et al. demonstrate that the sona of a given interrogation pulse is significantly longer than the pulse that generated it [8]. This stands to reason, given that the sona represents reflections of the initial pulse shifted in time by differing path lengths.

The reverse is also true: A time reversed sona will generate a reconstruction that is significantly shorter than it in time. This trait imposes a limitation on the ability of time reversal to transmit power. However, transmitting multiple sonas at once from the same antenna is possible—copying and shifting the signal in time can allow more data to be sent in one transmission cycle. This will in turn result in multiple transmitted reconstructions, and improved power transmission.

A concern with the above method is whether or not it would result in lost information. Sonas are sinusoidal signals—if overlaid, they will interfere constructively and destructively. Destructive interference may result in the “deletion” of transmission paths, reducing the fidelity of the created reconstructions.

### 4.2 Methodology

This test sought to test the practicality of overlapping sonas as a method of transmitting power. This experiment was done using the linear time reversal setup described

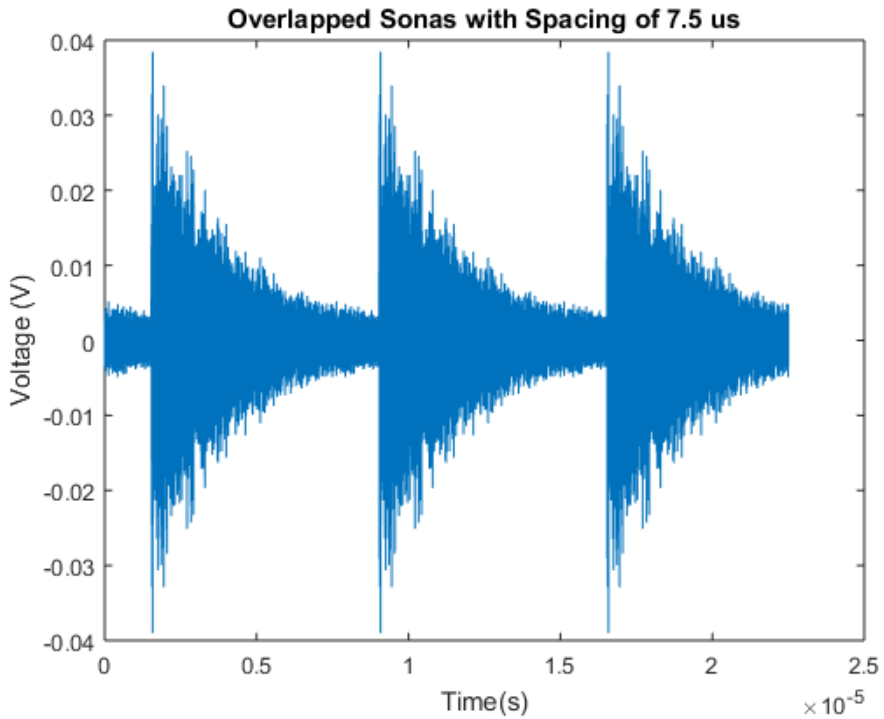


Figure 4-1: Overlapping sonas with a spacing of  $7.5 \mu\text{s}$ .

in Section ???. A sona was generated connecting a given starting and ending point. To prove that the sona could converge on the target, it was time reversed without any further manipulation, and the reconstruction was measured.

Once the efficacy of the sona was established, overlapping sonas were created. Overlapping sonas were created by copying and evenly spacing the original sona in time across the broadcast window, or the span of time over which the signal was broadcast. Figure 4-1 gives an example of sonas overlapping in this way. The overlapping sonas were time reversed and broadcast through the linear system in the same manner as before, which resulted in the reconstructions in Figure 4-2.

### 4.3 Results

Sonas were tested with offsets between  $0.1 \mu\text{s}$  and  $15 \mu\text{s}$ , by increments of  $0.1 \mu\text{s}$ . The average peak to peak voltages of reconstructions created with these sonas are plotted in Figure 4-3. Note that increasing the number of sonas increases the amount

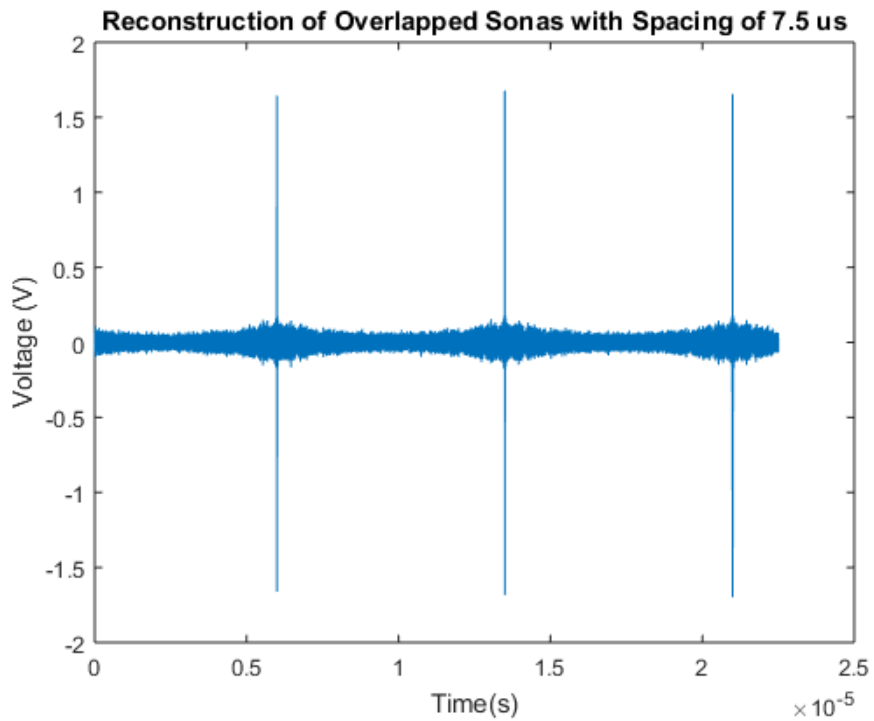


Figure 4-2: Reconstructions resulting from the sonas in 4-1.

of power transmitted in a given time frame. As such, the trend observed in Figure 4-3 is a result of the internal power settings of the PSG.

## 4.4 Discussion

TODO:Needs to be filled out.

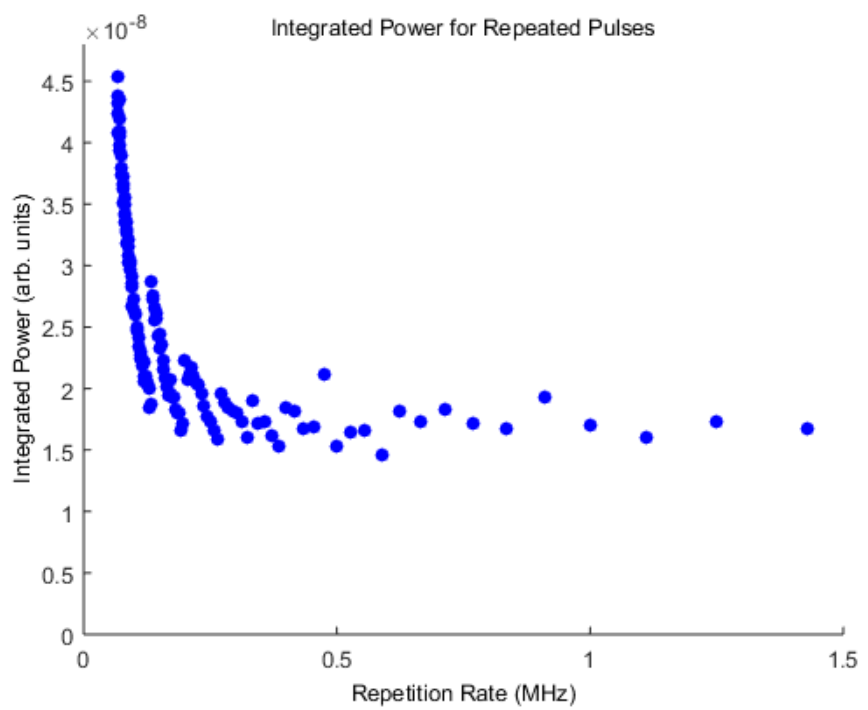


Figure 4-3: Integrated power from overlapping reconstructions.

# Chapter 5

## Spatial Profiling

TODO:...



# Chapter 6

## Moving Reconstructions

TODO:...



# Chapter 7

## Methodology for Conducting Nonlinear Time Reversal

The preceding chapters have been concerned with linear time reversal, or LTR, and have focused primarily on investigating properties of reconstructions. Now, we move into our nonlinear/NLTR investigations, which focus on proof of concept of targeting capabilities. As a reminder, NLTR makes use of harmonic reflections from the target to isolate it via frequency domain inspection after the sona is collected, a process similar to how we would envision a TR based WPT system to work.

Conceptually, our general process is this: we broadcast a Gaussian pulse from one port serving as both the transmitter and the receiver. Elsewhere in the Giga-box is a nonlinear element serving as a target. Any reflections from this element will contain harmonics: frequency components at multiples of the original frequency. These harmonics are embedded along with all the other echos in sona collected back at the transceiving port. However, before time reversing the sona, we transform it into the frequency domain and filter out all the components not within some band of the harmonic frequencies. In this way, we isolate only those wave paths that had contact with the nonlinear target. That filtered sona is time reversed and rebroadcast from the transceiving port, which will cause a slightly distorted version of the original Gaussian pulse to reconstruct at the target. This process is illustrated in Figure 7-1.

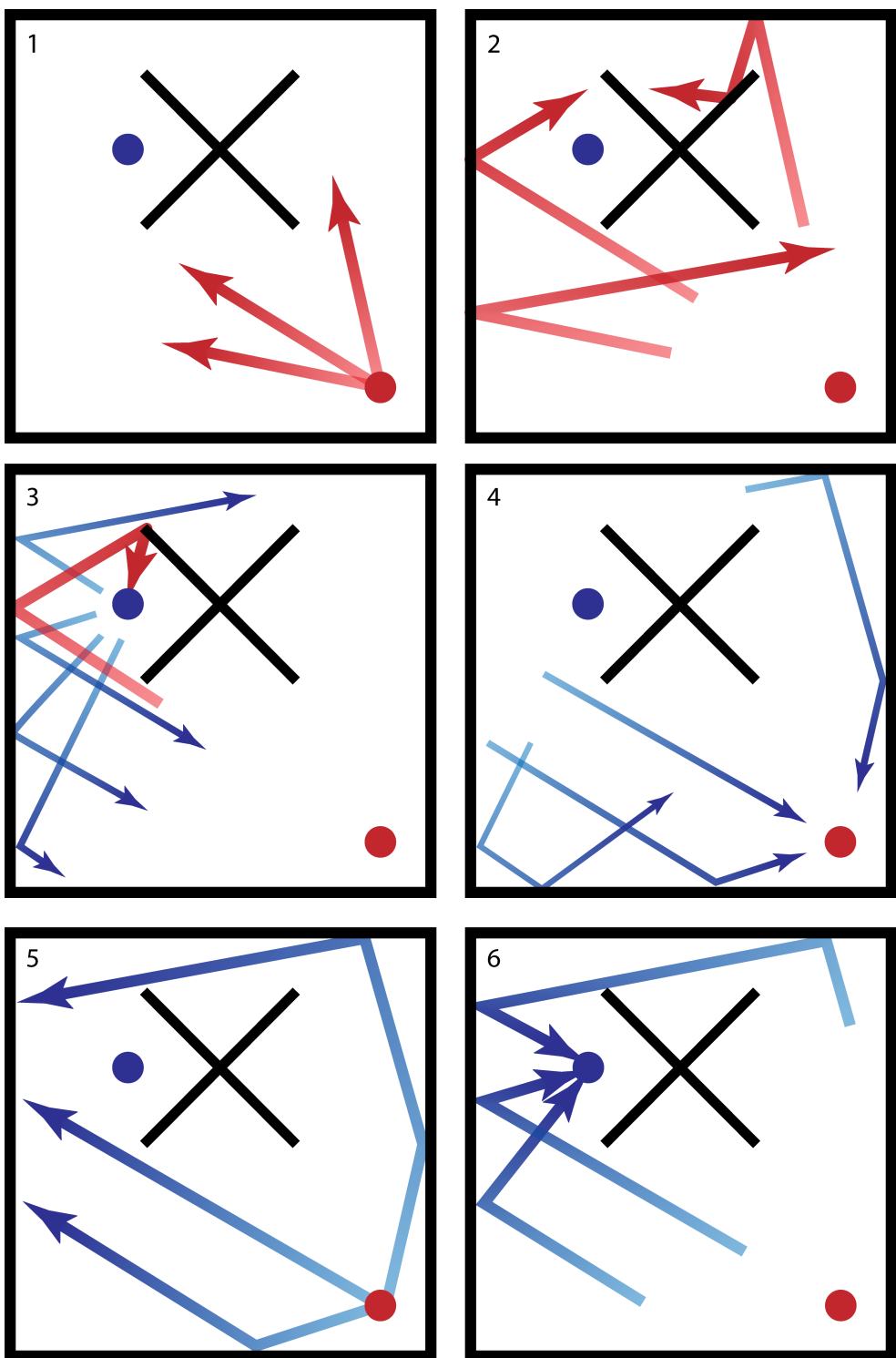


Figure 7-1: Reading order from top left: 1) The TRM broadcasts a signal into the cavity at one frequency, which 2) reverberates within the cavity. Eventually, 3) the signal reaches the nonlinear element somewhere within the chamber. Reflected waves that encounter this element will have a characteristic frequency signature containing harmonics of the original signal. 4) Some of these harmonic reflections will find their way back to the TRM. the TRM filters the sona to extract only those reflections, then time reverses and 5) re-emits them. 6) The time reversed waves collapse back on the nonlinear target.

# Chapter 8

## Using Nonlinear Time Reversal for Selective Reconstructions

TODO:Bring this over from google doc.



# Chapter 9

## Numerical Simulations of the Nonlinear Time Reversal Process

### 9.1 Purpose

In this chapter, we focus entirely on numerical simulations of NLTR as they apply to WPT. Our focus was threefold: (1) simultaneous NLTR collapse onto two nonlinear objects simultaneously (2) selective collapse of NLTR onto two distinct nonlinear objects and (3) characterize the transmission efficiency of the process. From these three focuses, we showed the NLTR process may be generalized to an arbitrary number of nonlinear objects in an enclosure and that these reconstructions may be selectively rectified at the nonlinear objects. We provide a scheme to characterize the efficiency of our process but were unable to develop a theory for tuning the efficiency. Our results provide a fundamental baseline for developing an experimental algorithm for targeting objects in an enclosure for WPT applications, either selective or non-selectively. We will first discuss the general scheme used for performing NLTR followed by the setup, experimental results, and discussion for each of our three focus topics.

The process of developing a new technology required benchmarking each step diligently. Any successful WPT technology must have very high effective transmission efficiency, implying minimal loss in each step of the system. Given the broad frequency signals used in experimentation, a significant drawback to any TR experiment is

the inherent wave reflection at interfaces between equipment, various mediums, or circuitry [23, 12]. While wave reflection losses can be theoretically be measured via S Parameters (explained later) of an experiment, these sources of loss are not practically measurable due to the fact that measuring the losses would create addition interfaces in the system, introducing additional sources of wave reflection [23]. To calculate the true ceiling on effective transfer efficiency, it is necessary to numerically simulate the process, as a simulation can calculate the various losses without interfering with the system itself.

In addition to using simulations to study the sources of loss in our system, it also provided us with a simple nonlinear element—a model diode. As explained in previous chapters, the nonlinear response of in our Gigabox experiments was found to be difficult to excite due to power limitations, noise, or equipment sensitivity. The difficulties that we encountered in our physical experimentation were circumvented by numerical simulating the NLTR process. By being able to monitor the voltage and current response of the diode at all times in the simulation, we were able to troubleshoot problems that occurred in the numerical NLTR process that would have otherwise have been impossible to determine in experimentation.

## 9.2 Methodology

### 9.2.1 Equipment

In order to perform these tests that were not possible in the Gigabox, we used the program Computer Simulation Technology: Microwave Studio (CST for short) to perform electromagnetic wave simulations. CST is an industry standard modeling program that uses the Finite Integration Technique (FIT) to numerically solve Maxwell's equations [26]. This technique is a generalized version of the well-known Finite Difference Time Domain (FDTD) method but can resolve complex geometries and boundary conditions in a simpler manner. We will not discuss these techniques at length, as they are well-understood in the literature [21, 29]. Our team had two computers with

a total of two shared CST licenses to perform simulations. The processing power, RAM, and GPU availability are shown below in Table 9.1. CPU A was used for either single simulations or computationally small simulations. A single simulation refers to a simulation where we did not sweep a parameter. CPU B was used for large simulations or parameter sweep simulations, requiring either large amounts of memory or large amounts of time, respectively. In general, we used CPU A to perform NLTR and selective NLTR while we used CPU B to calculate transfer efficiency and characterize nonlinear response characteristics.

	<b>CPU A</b>	<b>CPU B</b>
Processor	Intel Xeon CPU X5670 @ 2.93 GHz	Intel Xeon CPU E5-2680 @ 2.50 GHz
Number of Processors	2	2
RAM	44 GB	128 GB
GPU Available	No	Yes

Table 9.1: Technical specifications of the computers used for conducting all simulations and modeling.

### 9.2.2 Time-Reversal and Nonlinear Sona Extraction

To start any simulation, we first generated a Gaussian pulse signal in MatLab. For this interrogation signal, we chose the amplitude, center frequency, and bandwidth frequency for our experiment. An example input signal is shown inset in Figure 9-1. The simulation was run using this pulse signal, noting one of the ports as an injection port (e.g. Port A) and one as the recording port (e.g. Port B).

In general, we had two methods to extract the nonlinear sona from our recorded signal: (1) applying a Fourier transform and band-pass filtering the raw signal and (2) pulse inversion. As previously discussed, many of the Gigabox experiments were performed by recording a sona, applying a Fast Fourier Transform (FFT), and finally using a band-pass filter on the recorded signals to extract the harmonic signal at

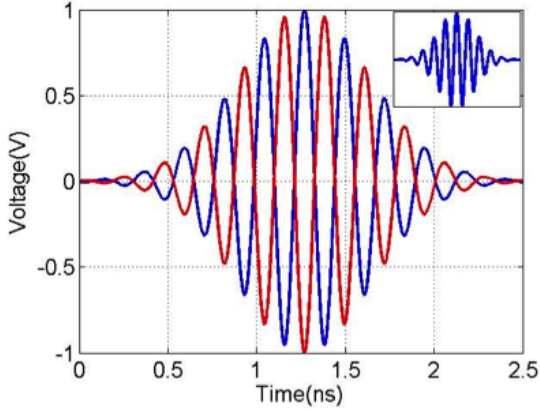


Figure 9-1: This shows our input waveform with a 4.4GHz center frequency and 1.0GHz bandwidth. The blue signal is the non-inverted input and the red signal is the inverted input. A singular, non-inverted waveform is shown in the inset.

the correct frequency. In our numerical simulations; however, the sonas were only recorded for 30–35 ns and the discretized nature of the data on this time scale led to distortion of the sona signals. The team also explored using another method of sona extraction that has been well documented in the literature [22, 14]. Hong et al. have used this method for numerous time-reversal experiments, citing its computational simplicity as a benefit for using it in physical experiments [14]. The process involves summing two signals, rather than applying a transformation to an entire sona signal, saving time. While this process proved to be very difficult for our Gigabox experiments, it was quite efficient at producing the nonlinear sona in CST. Due to the simplicity of pulse inversion, we used this method for extracting all nonlinear sonas. In this method, we ran the same simulation once with our original input signal and then we ran it a second time with an inverted version of our original signal. Inversion simply means that the entire original signal was multiplied by  $-1$ . Assuming a linear system, the sum of the original and inverted signals sums to 0; however, a nonlinear system sum is non-zero. Because the diode is the only nonlinear portion of the system, summing the original and inverted signals yields only the signal from the diode, which is the desired nonlinear sona. **TODO:Need to annotate figure with a,b,c,d** Figure 9-2(a) and (b) illustrate two sona signals, where the blue signal is the non-inverted sona and the red signal is the inverted sona. Figure 9-2(b) contains a

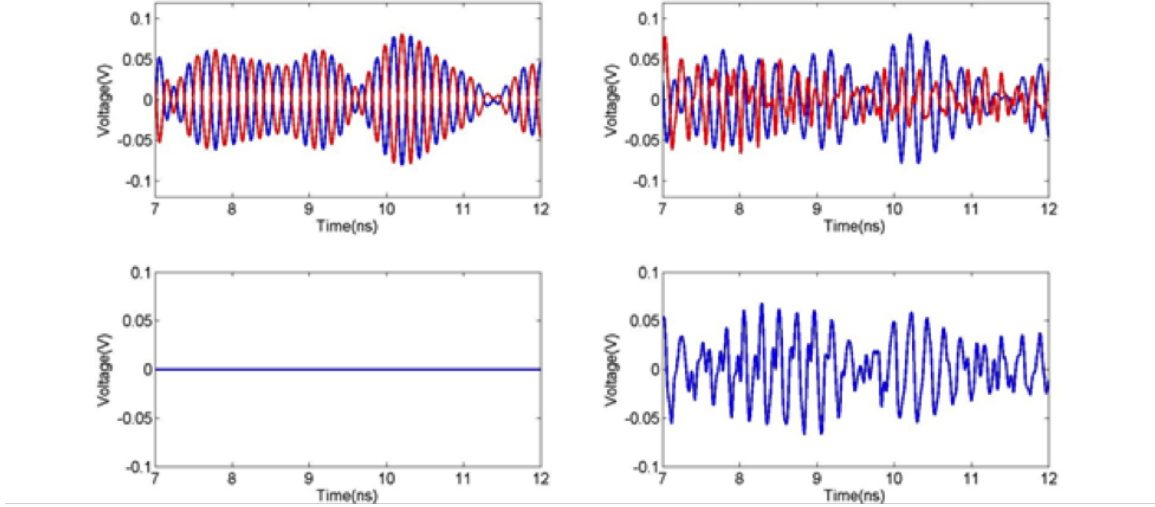


Figure 9-2: (a) shows a portion of the non-inverted (blue) and inverted (red) recorded response signal. (b) shows the same two response signals when a diode is present in the simulation. (c) the sum of the two signals in (a), resulting in signal annihilation. (d) the sum of the two signals in (b), which produce a non-zero signal.

nonlinear element while 9-2(a) does not. The corresponding (c) and (d) show the result of summing the two signals. It is clear that total annihilation of the sona signal occurs when no nonlinear element is present, as in 9-2(c), while a clear signal is present in 9-2(d).

This method to extract the nonlinear sona was chosen over taking the FFT and filtering the recorded signal as sample rate for the simulation data was not high enough to ensure the results would not be distorted. This discretization of data caused the resulting time-reversed sonas to produce incorrect results using the FFT and filter method, while the time-reversed sonas produced correct results with the pulse inversion method.

### 9.2.3 Defining and Controlling the Nonlinear Element

In the simulations themselves, we used a model diode as our nonlinear object, as it has a nonlinear I-V curve. The diode location for each simulation was chosen semi-arbitrarily with the only restriction to not be within 1–2 wavelengths of either port, as this may have created near-field effects that influenced the results. In CST, the diode component is modeled as the following circuit (Figure 9-3) and mathematical

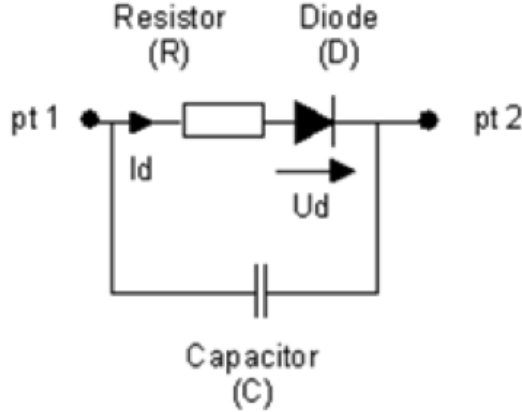


Figure 9-3: CST circuit model of a diode.

relationship (Equation 9.1 and 9.2). From these, the user may change the parasitic capacitance ( $C$ ), the series resistance ( $R$ ), the reverse conductance ( $G_s$ ), and the functional temperature ( $T$ ).

For  $V_d > 0$ :

$$I_d = I_0 \left( e^{\frac{eV_d}{kT} - 1} \right) = I_0 \left( e^{\frac{V_d}{V_k} a - 1} \right) \quad (9.1)$$

For  $V_d < 0$ :

$$I_d = G_s V_d \quad (9.2)$$

To obtain idealized results, we set  $C$  and  $G_s$  to 0, as these values reduced the magnitude of the nonlinear response. We used the default  $R = 50\Omega$ , as very large  $R$  reduced the overall signal greatly and a very small  $R$  did not produce any harmonics. This left only  $T$  to tune the I-V curve of the diode. In real life, different diodes have different I-V curves based on material. In order to simulate these differences mathematically, we changed the temperature of the diode in the simulation, as shown in Figure 9-4.

In reality, this changed the knee voltage ( $V_k$ ) for the diode. We chose  $V_k$  to be the applied voltage needed to achieve a current of  $0.2I_0$ . The parameter  $a$  is used to define this  $0.2I_0$  cutoff. As discussed later in this chapter, we will show how the nonlinear response of a diode is dependent on both the input pulse amplitude and the

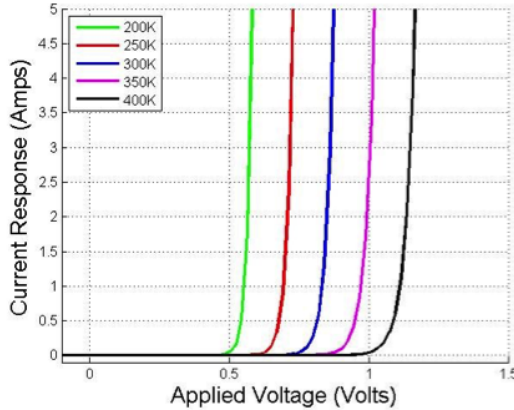


Figure 9-4: Different I-V curves that can be modeled in CST. It should be noted that the “Temperature” of the diode only changes its mathematical definition of the I-V curve

knee voltage. This nonlinear response was maximized to allow for selective targeting between two diodes simultaneously.

## 9.3 Results

### 9.3.1 Simultaneous Nonlinear Time Reversal

The first focus of our numerical simulations was to illustrate the collapse of time-reversed nonlinear sonas on multiple targets simultaneously. To be an effective WPT system, our technology would need to be able to charge more than one device at a time. Based on literature illustrating NLTR collapsing on a single nonlinear object, we hypothesized that a nonlinear sona would collapse on an arbitrary number of nonlinear objects if the nonlinear objects were present in the time-forward step of NLTR [9, 8]. We assumed that the reconstruction on each nonlinear object would sum linearly and independently such that no reconstruction would interfere with another, as shown in Equation 9.3, where  $R_i$  is the reconstruction on a single nonlinear object and  $x_i$  is a weighting of the amount of power that the single nonlinear object contributes to the overall power of all reconstructions. Based on this, we expected the reconstruction waveforms of the independent single-diode simulations to match a single, multi-diode

simulation.

$$R_{tot} = \sum_i R_i x_i \quad (9.3)$$

This feature was realized by creating a geometry with two diodes present along with two ports to record and emit signals, shown below. We created a quasi-two-dimensional (2D) irregular cavity in CST. This cavity was a 15cm x 15cm x 0.76cm square box modified with various circular and elliptical segments removed from the walls as shown in Figure 9-5. The 0.76cm height was chosen to maintain a 2D simulation. Equation refeq:numerical-cutoff-freq was used to calculate the cutoff frequency for the fundamental mode of a parallel plate cavity, below which only 1 frequency will propagate, reducing the time needed to simulate [12].

$$f_c = \frac{c}{2h} \quad (9.4)$$

Using a cavity of height 0.76 cm resulted in a cutoff frequency of 20 GHz, well above our typical test frequencies of 4-5 GHz fundamental and 8-10 GHz harmonic. We chose this cutoff frequency in the event we needed to use a higher fundamental frequency to create better spatial resolution of our reconstruction. The area dimensions for the Cut Box Model were chosen to minimize computational time while still maintaining a reasonable mode density, as shown in Figure 9-5(a)TODO:need to annotate figure. This mode density is required to allow the ray chaotic environment to have high sensitivity to initial and boundary conditions; a low mode density will prevent NLTR from having high spatial resolution.

We used two Teflon-coated dipole antennas to emit and record signals [13]. Two diodes are placed inside the cavity, shown by the blue circles in Fig. 5. A 4.4 GHz center frequency pulse with a 1.0 GHz bandwidth was chosen to minimize the reflected power and applied to antenna A. The interrogating pulse is shown as an inset in Figure 9-5(a).

The specific frequency and bandwidth was chosen for this geometry to minimize initial wave reflection ( $S_{11}$ ) into the enclosure. Figure 9-6 shows that using a 1

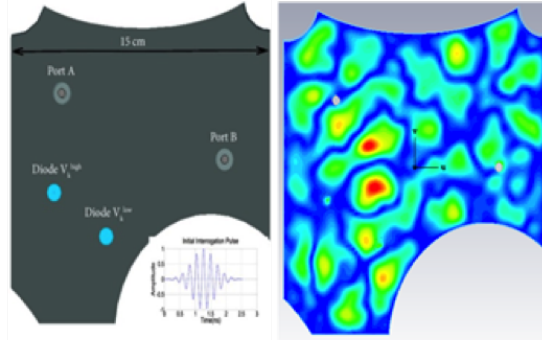


Figure 5: The cut-box simulation geometry used in CST. (a) shows the location of the 2 ports (A and B), 2 diodes ( $V_k^{high}$ ,  $V_k^{low}$ ), length scale, and the lower inset shows the initial interrogation pulse. (b) shows the electric field at a point in the simulation, illustrating the limited excited mode density.

Figure 9-5: The Cut Box simulation geometry used in CST. (a) shows the location of the 2 ports (A and B), 2 diodes ( $V_k^{high}$ ,  $V_k^{low}$ ), length scale, and the lower inset shows the initial interrogation pulse. (b) shows the electric field at a point in the simulation, illustrating the limited excited mode density.

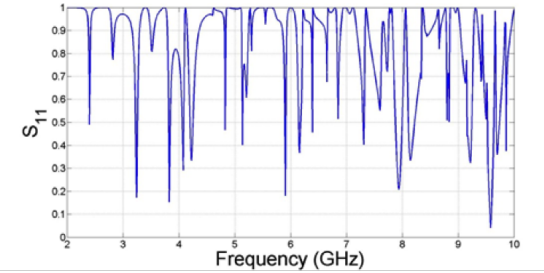


Figure 9-6: The  $S_{11}$  spectrum for the Cut Box Model. We wanted to minimize  $S_{11}$  for our simulation while maintaining a large bandwidth. This led to choosing a 4GHz center frequency with a 1GHz bandwidth.

GHz bandwidth, an optimal center frequency is 4.4 GHz. The dips in the  $S_{11}$  value represent optimal frequencies to use, as a low  $S_{11}$  indicates a large portion of the signal entered the cavity. The large number of peaks is indicative of the mode density of the geometry, where low frequencies are sparse given the relatively small scale of the cavity.

Using this input pulse and the pulse inversion method of sona extraction, we were able to perform NLTR in the Cut Box Model. By measuring the observed voltage and corresponding current during the time-reversed step, we measured the quasi-power over time in each diode. As shown in Figure 9-7, the reconstruction waveform on

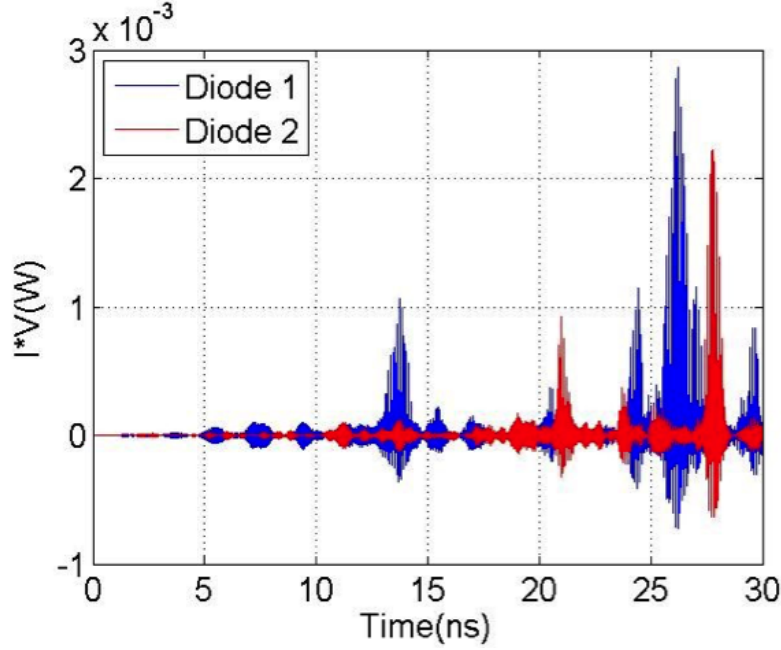


Figure 9-7: The time-reversed reconstruction on two diodes simultaneously performed inside the Cut Box geometry.

each diode matches the expected results for a 1-diode experiment [25, 4].

### 9.3.2 Discussion of Simultaneous Nonlinear Reconstructions

This result alone signifies the generality of NLTR whereby any nonlinear object in the cavity will observe a reconstruction in the time-reversed step. In regards to a larger WPT system, one can imagine that this is particularly useful inside of a home or public area, where any device may be powered as long as it is within range of the transmitter/receiver base station. Because the process used only creates a reconstruction at the nonlinear element, it is as simple as repeating the NLTR process rapidly, creating a quasi-pulse width modulation (PWM) signal that can charge a battery. PWM is a method for controlling how active a device is by rapidly switching the device on and off. For example, a fan has different speeds because it operates 25%, 50%, 75%, or 100% of the time. Similarly, if we can reconstruct on a battery circuit every 10% or 20% of the time, we can effectively charge the battery. As soon as the nonlinear object leaves the enclosure, it will no longer receive power. By having a base station that can actively modulate output sona power, it would be very simple to

change the amount of power transferred to each device. This dynamic power control is outside the scope of our project but represents a much later extension to this WPT system.

### 9.3.3 Simulation of Selective Collapse of NLTR

The logical next step is to determine how such a system would be able to determine which device should be powered. As previously shown, if nothing is done to alter the sona signals, then the sona from each nonlinear object will sum linearly and produce reconstruction at all nonlinear objects in the time-reversed step. Given that each reconstructions sums independent of one another, we hypothesize that we should be able to eliminate the contribution of one nonlinear reconstruction to the overall set of reconstructions without altering the fidelity of the any other individual reconstruction on other nonlinear elements. For example, in an enclosure with 3 diodes, if we could suppress the response of diode 2 in the time-forward step, then we would expect to only observe a reconstruction on diodes 1 and 3, creating a selective targeting method.

Using Eq. 3, this would imply a weight of  $x_i = 0$ , as shown in Equation 9.5.

$$R_{tot} = \sum_i R_i x_i = R_1 x_1 + R_2 x_2 + R_3 x_3 \quad (9.5)$$

TODO:How does this imply  $x_i=0$ ?TODO:why does this stop at 3 specifically? Should it go on to  $x_i$ ? If so we need  $2 + \dots + i$ .

In a commercial setting, this would be an extremely useful aspect to our WPT system, as companies could require payment to use the system and would otherwise suppress the reconstruction on the user's device. The fact that the nonlinear object is passive in the environment implies that this selective targeting could even be used to "resurrect" a dead phone, a feature not seen on any current WPT technology on the market.

We have developed a method of performing such a targeting scheme based on the previously mentioned diode model. In the simplest case, we show that selective targeting for 2 diodes with two separate voltage knees was obtained (noted  $V_k^{high}$  and

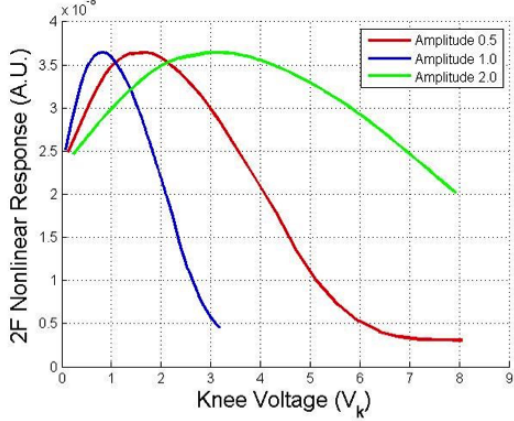


Figure 9-8: The nonlinear response of the diode had a clear maximum at a specific knee voltage. By using a pulse amplitude that corresponded with the specific diode knee voltage, we could selectively target diodes in CST.

$V_k^{low}$ ).

Recall the current response in the diode from Equation 9.1. One useful aspect to the diode definition function is that if  $V < V_k$ , then the diode has very little current response, which in turn implies a low nonlinear response. We utilize this characteristic while performing selective targeting on a low  $V_k$  diode. Similarly, we observe that at small  $V_k$  values, the nonlinear response is small. These two observations led to the hypothesis that nonlinear response may be maximized given an initial pulse by selecting a proper  $V_k$  value. As shown below, Figure 9-8 was obtained by sweeping over many  $V_k$  values for different initial pulse amplitudes given the same geometry and process conditions as previously stated. Given this distribution, we may target a high  $V_k$  diode, as the nonlinear response will be stronger in the high  $V_k$  diode than the low  $V_k$  diode.

To perform this selective targeting, we once again used the Cut Box Model. In the simplest case, we consider selective targeting of a low  $V_k = 0.79V$  ( $V_k^{low}$ ) diode at the exclusion of a high  $V_k = 6.60V$  ( $V_k^{high}$ ) diode. Given the large value of  $V_k^{high}$ , we expect to see no response in that diode while maintaining a reasonable nonlinear response in the  $V_k^{low}$  diode. We used a pulse with amplitude  $V = 1.0V$  during the time forward step, emitted at Port A in Figure 9-5(a). Using pulse-inversion, we extracted the nonlinear sona from the recorded signal at Port B, time-reversed the signal, and

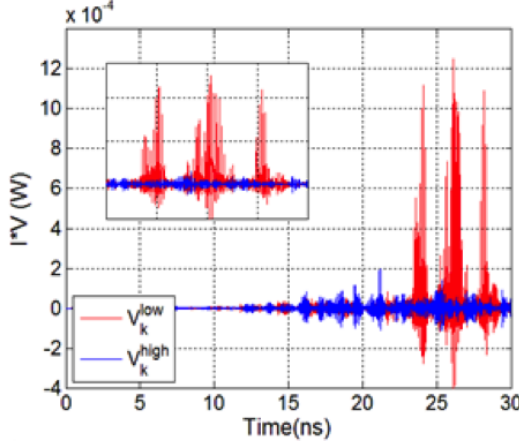
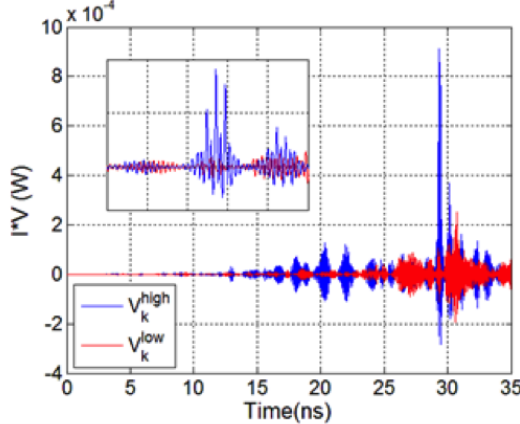


Figure 9: Time-reversed reconstructions on the two diodes while targeting  $V_k^{low}$ . Very little signal is seen on the  $V_k^{high}$  diode. The insert shows the details of the reconstructions between 22 and 30 ns.

Figure 9-9: Time-reversed reconstructions on the two diodes while targeting  $V_k^{low}$ . Very little signal is seen on the  $V_k^{high}$  diode. The insert shows the details of the reconstructions between 22 and 30 ns.

re-emitted it from Port B. Figure 9-9 shows the time-reversed reconstructions on both diodes. This results in a reconstruction almost exclusively on the  $V_k^{low}$  diode during the time-reversed step. The presence of three reconstructions when only one initial pulse was TODO:missing is not alarming, as short-orbit paths between Port A, the diodes, and Port B that carry enough power to excite the diode harmonics are known to exist [?]. To calculate the quality of the selective reconstruction, we determined the aspect ratio by comparing the max of  $IV$  on both diodes. For this scenario, we calculate a power delivery aspect ratio of 6.35:1 for the  $V_k^{low}$  diode relative to the diode with  $V_k^{high}$ .

The more difficult scenario was to selectively target a high  $V_k$  diode at the exclusion of a low  $V_k$  diode. We utilized the peak in nonlinear response as a function of knee voltage from Figure 9-8. By choosing the correct pulse amplitude corresponding to a peak value that was matched to the high  $V_k$  value, we expected to see the strongest nonlinear response from that specific diode, resulting in a stronger reconstruction. In this scenario, the low  $V_k$  diode will still observe a reconstruction; however, it will be smaller in amplitude than the high  $V_k$  diode reconstruction. Given that a real system would involve a rectification circuit in addition to the diode, the smaller amplitude



**Figure 10:** Time-reversed reconstructions on the two diodes while targeting  $V_k^{high}$ . Sona amplitude modulation resulted in a clear contrast between the two signals.

Figure 9-10: Time-reversed reconstructions on the two diodes while targeting  $V_k^{high}$ . Sona amplitude modulation resulted in a clear contrast between the two signals.

reconstruction may not be able to turn on the rectifier while the high amplitude reconstruction at the high  $V_k$  diode would turn on. For our simulations, we were able to model this by measuring the observed power ( $IV$ ) on the diode and modify the sona amplitude in order to ensure the  $V_k^{high}$  diode had rectification while the  $V_k^{low}$  diode did not.

For this second scenario, with  $V_k^{high} = 2.22V$ , we once again used an amplitude 1.0V pulse during the time-forward step so that we may compare the results from both scenarios equally. As shown in Figure 9-10, pulse amplitude of 1.0 has a maximum nonlinear response at 2.22V. We chose this  $V_k$  value, as it gave the clearest reconstruction. Once again, we used pulse-inversion to extract the nonlinear sona. In general, this results in a larger magnitude reconstruction on  $V_k^{high}$ . This contrast between the  $V_k^{low}$  and  $V_k^{high}$  reconstructions was amplified by modulating the time-reversed sona amplitude, such that the reconstruction voltage seen at the target diode was barely larger than  $V_k$  for  $V_k^{high}$  and just barely smaller than  $V_k$  for  $V_k^{low}$ . This resulted in selectively reconstructing on  $V_k^{high}$  only during the time-reversed step with an aspect ratio of 3.61:1 for the  $V_k^{high}$  diode relative to  $V_k^{low}$ , as shown in Figure ??TODO:Which ref?.

### **9.3.4 Discussion of Selective Nonlinear Time Reversal**

We have demonstrated a basic method for creating selective rectification using NLTR to target different nonlinear objects. This represents a stepping stone from the previously shown method of generalizing NLTR. By altering the input pulse amplitude, we were able to achieve the hypothesized nonlinear response suppression of specific nonlinear elements. This shows that the nonlinear reconstruction created on each nonlinear element is independent of one another and may be modified without impacting the other elements of the overall reconstructions. We have shown that this WPT technology would be capable of ubiquitous charging or any nonlinear device as well as selective targeting of specific devices. One may think of this as having an NLTR charger in one's home compared to having an NLTR in a business. In a domestic setting, there is very little need to restrict access to power. There are many outlets in one's home and there is no need to tell someone they are not permitted to use it. In a business however, a power outlet is not available to customers unless they pay for it. In this case, it is very useful to be able to selectively choose who may receive power. Although we have not shown a full-fledged system to do so, we have presented a foundational process that may be improved upon in order to create a successful NLTR-based WPT system.

### **9.3.5 Simulation of Transmission Efficiency of NLTR Process**

We have so far shown that NLTR may be used in a WPT system to either power all nonlinear objects or selectively target the nonlinear objects within a relevant range. One significant question though that arises is to what efficiency are these objects powered. Surely a system that can only transfer 2% of applied power will not be a successful WPT technology, as the consumer is paying for the luxury to not carry around a cable. If the user has to pay 50x more for the power they are very unlikely to use our system. As previously discussed, energy losses are often difficult to calculate in real experiments due to wave reflection and other systematic sources of error. However, by simulating the NLTR process, we are able to observe approximate

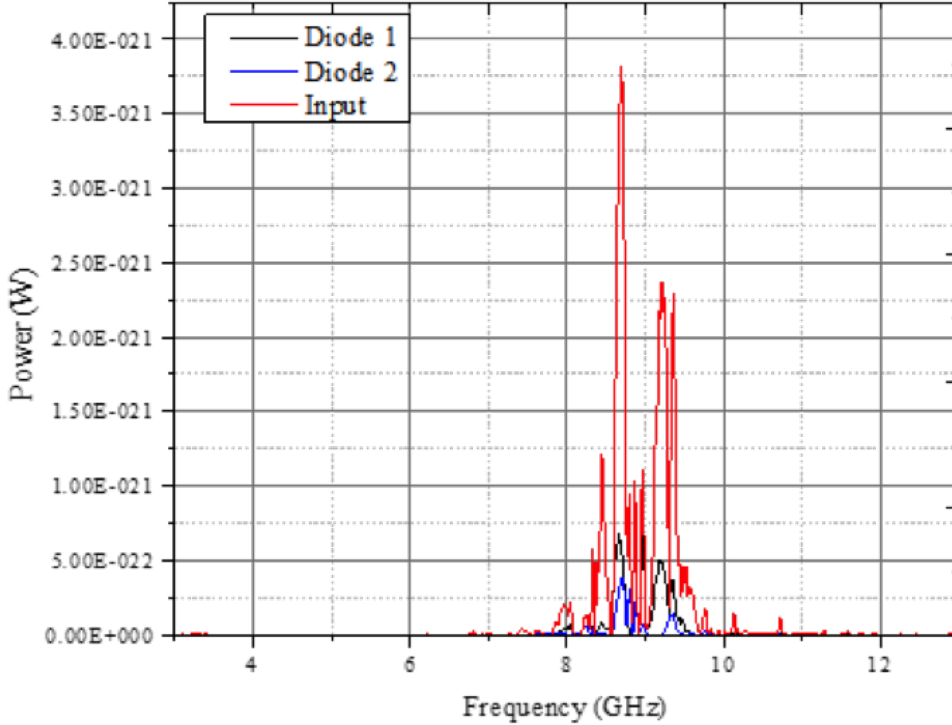
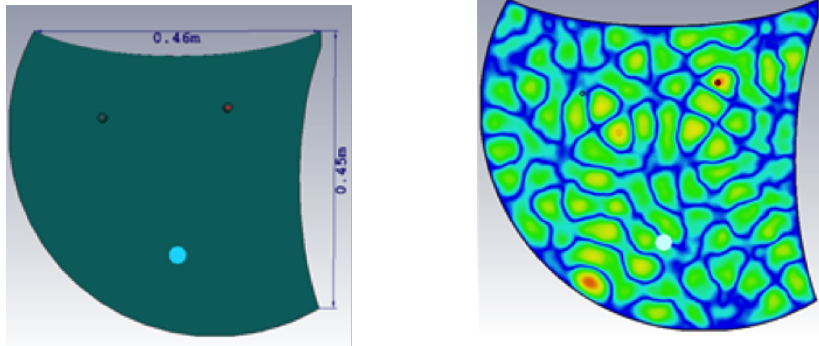


Figure 9-11: A typical power spectrum obtained in the time-reversed step (reconstruction). The power that enters the diodes only represents a portion of the overall power input in the simulation.

transfer efficiency. In CST, we are able to track power input and power loss via wave reflection, absorption in both lumped elements and environment materials, and radiation loss at another port. One drawback to using the built-in CST power tracking is that everything is recorded in the frequency domain rather than time domain. For example, a typical power spectrum from a time-reversed step of a 2-diode NLTR simulation is shown in Figure 9-11. As we are interested in overall power input compared to overall power output, we used this data along with Equation 9.6 to compute the efficiency of transfer in our simulations.

$$e = \frac{\sum_i P_{i(diode)}(f)}{\sum_i P_{i(input)}(f)} \cdot 100 \quad (9.6)$$

The above data was taken from a simulation run in the Cut Box Model for the previously discussed two-diode simultaneous reconstruction. For this simulation, we found that 18.6% and 7.3% of power were transferred from the nonlinear sona to



(a) Illustrates the geometry of the room model.  
(b) Illustrates the relatively large mode density present in the simulation.

Figure 9-12: The room model

diodes 1 and 2, respectively. This provides a promising outlook.

Our next question was whether or not these transfer efficiencies were a function of distance between transmitter port, diode, and receiver port. We found that using similar diode positions as previously stated resulted in transmission values around the 7–18% shown above. We decided to introduce a new model with a much larger length scale, called the Room Model shown in Figure 9-12.

We chose to use a 45cm x 45cm x 0.76 cm initial box to simulate a large geometry while still maintaining a quasi-2D cavity. The 45 cm length scale was used, as any larger simulation would run out of memory. Due to the length of simulation and decreased nonlinear signal strength, this model was unable to be used for further efficiency calculations. From Figure 9-12, the distances in the simulation are much larger than the Cut Box and may be used in the future to determine whether transmission efficiency of NLTR is dependent on distance between transmitter, nonlinear object, and receiver ports.

## 9.4 Conclusion

Using CST, we have successfully demonstrated our 3 goals: (1) simultaneous reconstructions on multiple nonlinear objects (2) selective reconstructions between multiple nonlinear objects and (3) calculation of a baseline transmission efficiency of NLTR.

For simultaneous and selective targeting, we provide a basic framework to perform these processes using numerical simulations; however, these processes are still yet to be performed in real-world experimentation. We believe that this illustrates a foundational work for future experiments to demonstrate the feasibility of these features in a new WPT technology. Additional research must be done in order to characterize the ceiling on transmission efficiency if NLTR is to be applied to a future WPT technology.

# Chapter 10

## Nanorods

TODO:...



# Chapter 11

## Rectification

### 11.1 Goals of Rectenna

One of the main components of any WPT system is its rectifier, as it performs the crucial step of capturing the broadcasted energy and transforming it into a usable form. To accomplish this, a rectenna, a dual-purpose device that combines an antenna and a rectifier, is necessary. The antenna picks up the unusable, oscillating AC signal received from the transmitter, the rectifier converts the signal to relatively stable DC power, and this usable power is passed to an arbitrary load.

In addition to standard rectification, the rectenna must serve as a passive nonlinear element. In NLTR, a nonlinear element is required to produce harmonics from the initial interrogation pulse broadcast by the transmitter. However, this goal is secondary to the main purpose of rectification.

The rectenna was designed to fit the following parameters. First, the rectenna must operate efficiently at the high frequency (1–10 GHz) required for efficient NLTR. Additionally, losses due to reflection and parasitic effects within the antenna should be minimized. Finally, to fulfill the role of a nonlinear element, the rectenna should generate distinguishable harmonics strong enough for the purposes of NLTR.

In short, to rectify and generate harmonics for NLTR, the rectenna must be capable of not only efficient rectification at high frequencies, but also production of strong harmonics for NLTR.

## 11.2 Diode Selection and Testing

The diode is the most important single component to consider for the rectenna, as it is the main rectifying component. Careful consideration of its characteristics is vital. The switching frequency, forward voltage drop, and impedance of the diode are of particular importance to the desired goal of efficient rectification.

For the rectenna in our design to perform efficiently, the diode must satisfy several requirements:

The diode must maintain functionality as a diode at a transmission frequency of 1–10 GHz, and must rectify at a frequency of at least 10 GHz. This requirement severely limits the possible choices for the rectenna diode. The frequency of a diode is inversely related to its reverse-recovery time (TRR), the fastest time the diode can switch from forward to reverse bias [3]. In traditional P-N junction diodes, minimum TRR is on the order of tens to thousands of nanoseconds, even for fast diodes [7]. In a high frequency circuit, a P-N diode would be no different than a short circuit, and no rectification would occur.

The diode must have the lowest forward voltage drop possible. The voltage drop represents the reverse bias that remains when the diode works in the forward direction, and can be a significant contributor to power loss. The team's experimental WPT capabilities are limited to fairly low voltage microwave signals (.5 V to 1 V signal amplitude), which makes forward voltage drop especially important.

Finally, impedances should be minimized to reduce loss. All diodes have intrinsic impedances such as parasitic capacitance and resistance. Impedances contribute to losses during rectification and destabilize circuit behavior, resulting in unpredictable behavior.

Considering these factors, a Schottky barrier diode were chosen for the rectenna. Unlike P-N junction diodes, Schottky diodes have extremely low TRR and low forward voltage [7]. Schottky diodes do have a lower maximum reverse voltage rating, higher reverse leakage current, and higher cost than P-N diodes. However, these are relatively minor issues in our application. A Schottky MA4E1317 diode was used as the rectifying

diode. The diode parameters from the are shown in Table 11.1.

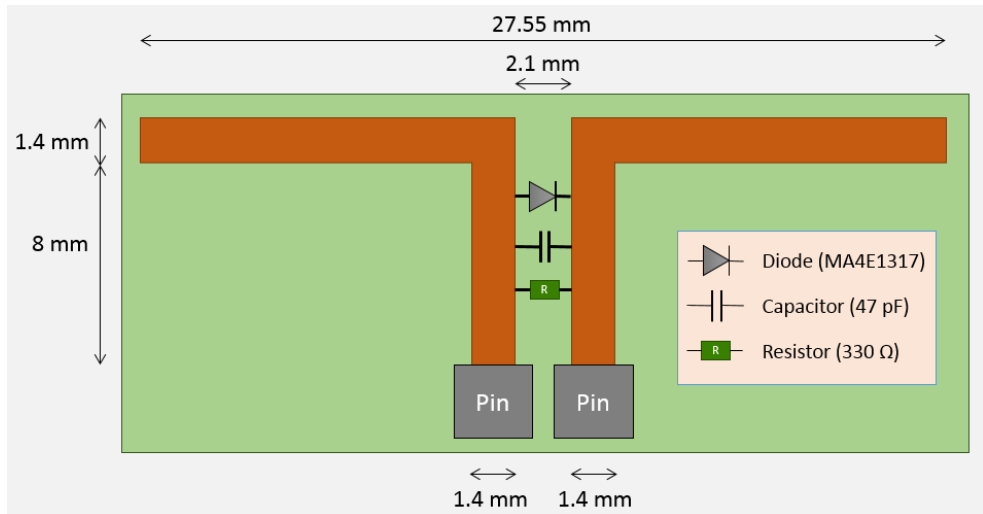
Test Conditions	Symbol	Units	Min.	Typ.	Max.
Junction Capacitance at 0 V at 1 MHz	C <sub>j</sub>	pF	-	.020	-
Total Capacitance at 0 V at 1 MHz	C <sub>t</sub>	pF	.030	.045	.060
Junction Capacitance Difference	D <sub>Cj</sub>	pF	-	-	-
Series Resistance at $+10\text{ mA}^2$	R <sub>s</sub>	$\Omega$	-	4	7
Forward Voltage at $+1\text{ mA}$	V <sub>f1</sub>	V	.60	.70	.80
Forward Voltage Difference at $+1\text{ mA}$	D <sub>Vf</sub>	V	-	-	-
Reverse Breakdown Voltage at $-10\mu\text{A}$	V <sub>br</sub>	V	4.5	7	-
SSB Noise Figure	NF	dB	-	6.5 <sup>4</sup>	-

Table 11.1: Datasheet for the M/A-Com MA4E1317 Schottky diode [17].

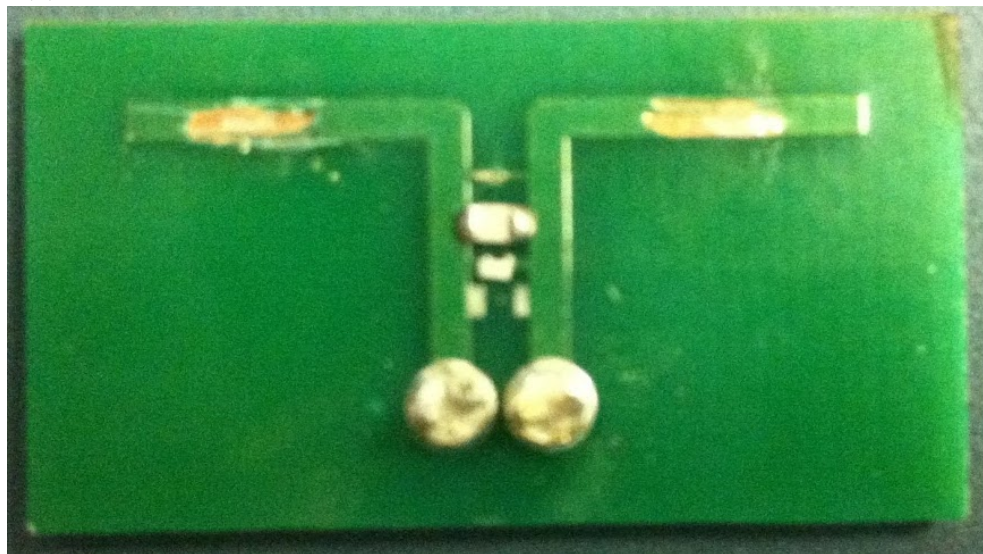
The MA4E1317 has low total capacitance (.045 pF) and series resistance ( $4\ \Omega$ ), minimizing parasitic losses. The datasheet also cites an operating frequency of up to 80 GHz for this diode, more than sufficient for our purposes. The forward voltage cited to be around .7 V, a typical value for most diodes [17]. A lower forward voltage would be desirable, and in considering future improvements to the system, this is definitely a point to consider.

### 11.3 Antenna Design

A printed circuit board (PCB) half-wave dipole was chosen as the antenna for the system. The copper trace acts as the antenna, and is etched into a FR-4 substrate. The MA4E1317 is a flip-chip device, and is only suitable for mounting on a PCB. The design and specific parameters of the antenna is based off of the dual frequency WPT rectenna in [24], but has been modified in our implementation. The design of the rectenna is shown in Figure 11-1.



(a) A schematic of the PCB rectenna design and component specifications.



(b) Image of the assembled rectenna

Figure 11-1: Rectenna design

The rectenna is composed of the MA4E1317 diode, a 47 pF ceramic capacitor acting as a low-pass microwave filter, a  $330\ \Omega$  load resistor, and output pins for measurement purposes. The antenna is designed for operation at 5.45 GHz, so the length of the dipole is 27.55 mm, half the wavelength of the incident wave.

One important distinction for this rectenna design is the lack of filtering for higher-order harmonics. This feature is common in most rectennas, but is deliberately left out so that the antenna can generate nonlinear harmonics from the interrogation signal.

No special consideration for impedance matching between the antenna and the rectifier components. This is definitely a point to consider for future improvement, as proper matching of the components should significantly improve the efficiency of rectification.

## 11.4 Rectenna Testing

To thoroughly test the rectenna, distinct tests were run to order to verify both its rectification and harmonic generation capabilities. We examined a range of frequencies for all tests to isolate peak performance.

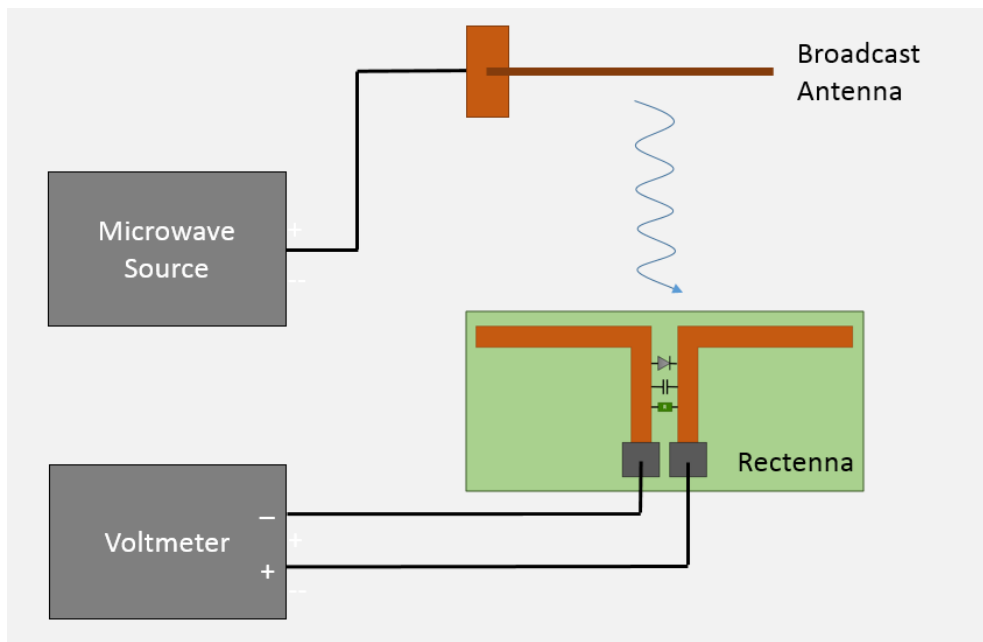
### 11.4.1 DC Power Characterization

To determine the overall rectification efficiency, a second antenna was used to broadcast energy to the rectenna. A 17 dBm CW signal was generated from the PSG and broadcast through a monopole antenna. The rectenna was then positioned parallel to the broadcast antenna, at a distance of 2 cm. and the average DC voltage and power was measured over the load resistor. The test was repeated over a range of broadcast frequencies from 1 to 7 GHz. The setup is shown in Figure 11-2a and the results are shown in Figure 11-2b.

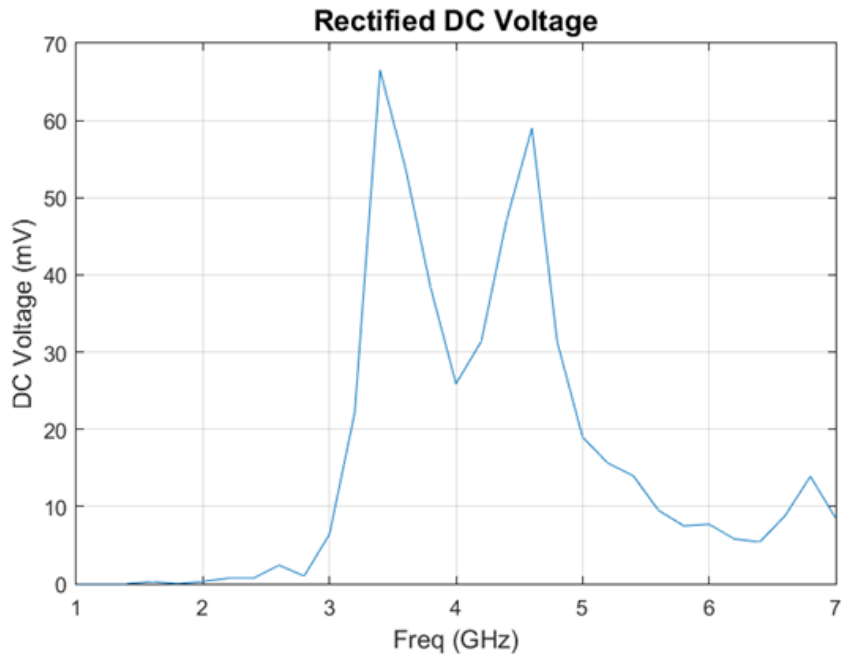
Rectification was most pronounced in the 3-5 GHz frequency band. Rectified voltage is highest at 3.4 GHz and 4.6 GHz, with DC voltage levels of 66.5 mV and 59.0 mV respectively. Unfortunately, DC voltage results of higher frequencies were unreliable and erratic given the measurement techniques, and accurate data could not be taken.

Given the resistive load of  $330 \Omega$ , rectified DC power can be calculated from the voltage above. Using DC voltage ( $V$ ) and load resistance ( $R$ ), the DC power ( $P_{dc}$ ) was calculated using Equation 11.1:

$$P_{dc} = \frac{V^2}{R} \quad (11.1)$$



(a) Experimental setup for rectification testing



(b) DC voltage measured from the voltmeter in the setup on the left for a range (1-7 GHz) of frequency inputs.

A plot of this is shown in Figure 11-3.

Considering the input power of 17 dBm (around 50.12 mW), the wall-to-load efficiency of the experiment is extremely low for all frequencies. These losses can come from a number of sources, including bad coupling between the broadcast antenna and

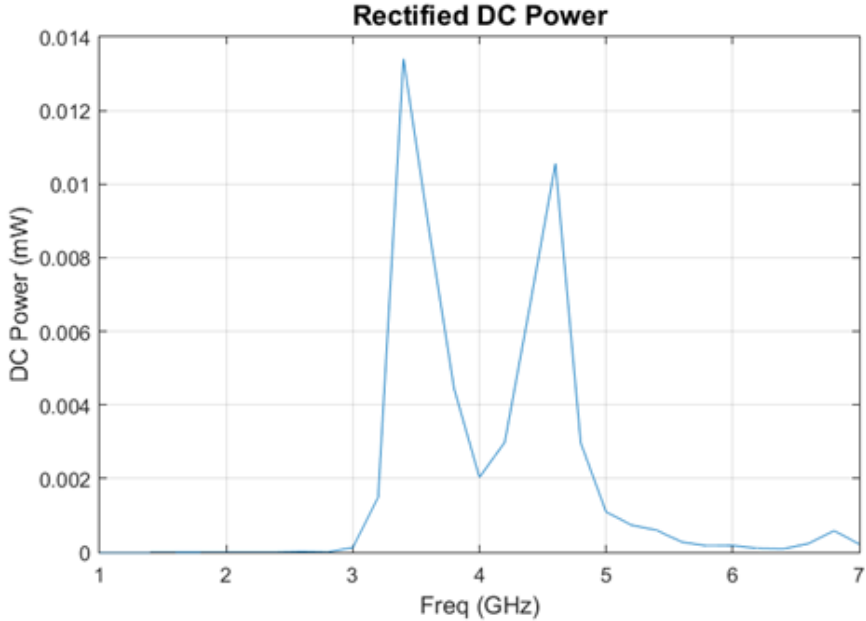


Figure 11-3: Rectified DC power calculated from DC voltage using the relation:  $P = \frac{V^2}{R}$

rectenna, reflection from broadcast antenna, losses in coaxial connections between components, and power radiated away from the rectenna, among others. However, the inherent losses of the experimental setup are not relevant to the overall efficiency of the system; for this, the efficiency result must be compared to only the rectification efficiency.

To establish rectification efficiency, AC power tests were conducted on a bare dipole antenna with no diode, resistor, or capacitor. The results of this test establish the overall power accepted by the rectenna, and is directly comparable to the previous DC power results.

The setup of the AC power experiment was similar to the DC power experiment, with the exception of two key differences: the voltmeter was replaced by a DS091304A oscilloscope, and the rectenna was replaced by the bare dipole antenna. In the absence of the  $330\ \Omega$  load resistor on the rectenna, the  $50\ \Omega$  input impedance of the oscilloscope [16] was used as the load.

Using AC voltage amplitude ( $V_{max}$ ) and load resistance ( $R$ ), the accepted AC

power ( $P_{ac}$ ) was calculated using Equation 11.2:

$$P_{ac} = \frac{V_{max}^2}{2R} \quad (11.2)$$

The setup and results of the test are shown below in Figures 11-4a and 11-4b, respectively.

Assuming that the transfer function between the antennas doesn't change between the AC and DC tests, these results allow the rectification efficiency to be calculated. The efficiency ( $E$ ) in this case is the ratio of the rectified DC power ( $P_{dc}$ ) to the total accepted AC power ( $P_{ac}$ ), as in Equation 11.3:

$$E = \frac{P_{dc}}{P_{ac}} \quad (11.3)$$

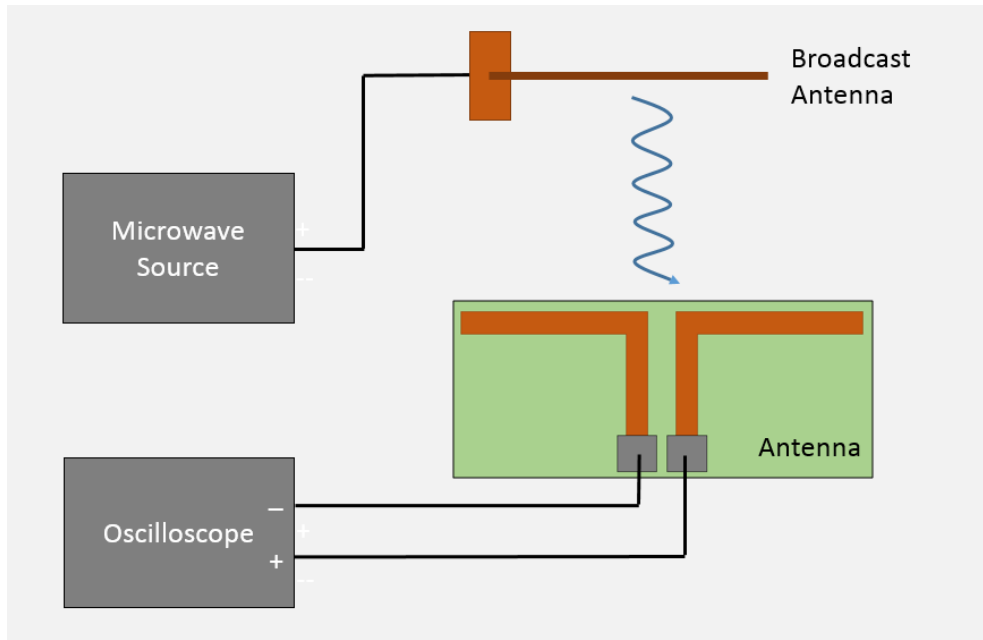
Figure 11-5 shows the efficiency calculated this way, across the range of frequencies tested.

Analysis of the graph shows the same peak rectification efficiencies at 3.2 GHz and 4.6 GHz, with 4.7% and 4.4% respectively. This rather low efficiency is expected given the lack of optimization and impedance matching in the rectenna. However, this result clearly demonstrates rectification of high frequency AC power.

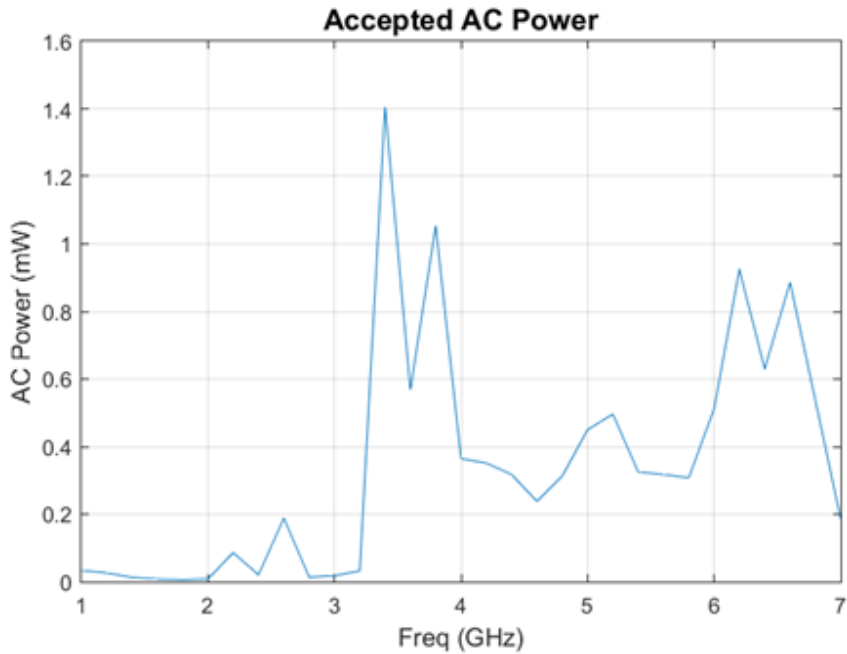
#### 11.4.2 Harmonic Generation

Harmonic generation was then tested by measuring second harmonic power reflected from the rectenna. The antenna was stimulated by a 0 dBm CW signal, and the second harmonic reflected from the antenna was collected using a directional coupler feeding into the spectrum analyzer for measurement. The test setup for and results are shown in Figure 11-6.

In initial testing, the harmonic generation of the rectenna was minimal, as the measured 2nd harmonic power was comparable to the noise level power. However, after filtering out harmonic responses from microwave source, a distinct 2nd harmonic was found at 2.45 GHz at -150 dBm compared to the noise level power of -161 dBm. Bandwidth restrictions of filtering components prevented analysis of a full frequency



(a) Experimental setup for measuring accepted AC power



(b) Accepted AC power, used to establish a baseline for efficiency calculation, calculated using the relation  $P = \frac{V_{max}^2}{2R}$ .

spectrum, and thus, 2.45 GHz is the only frequency we were able to probe for harmonics. Even so, this result does demonstrate the harmonic generation capabilities of the rectenna.

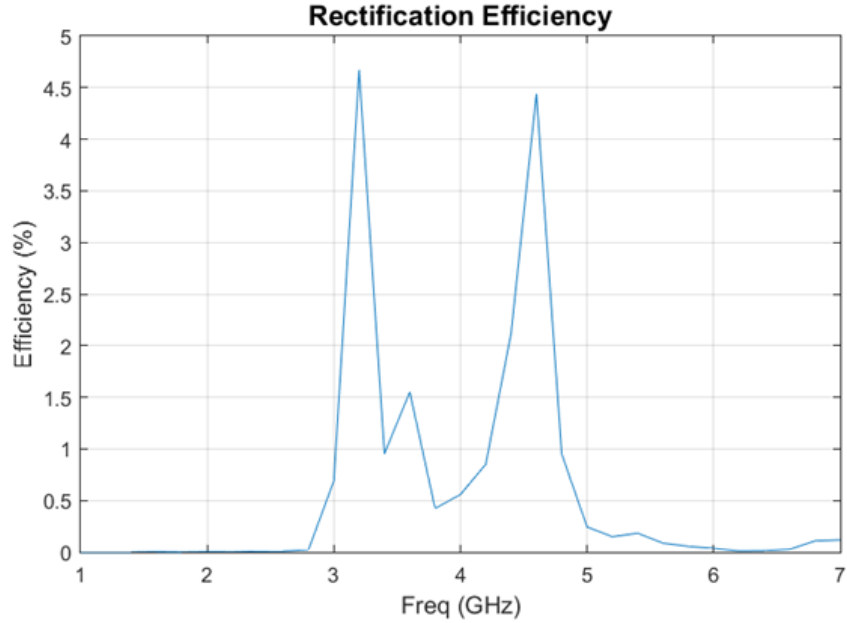


Figure 11-5: Rectification efficiency, calculated using accepted AC power as a baseline. Calculated using the ratio of rectified DC power to accepted AC power.

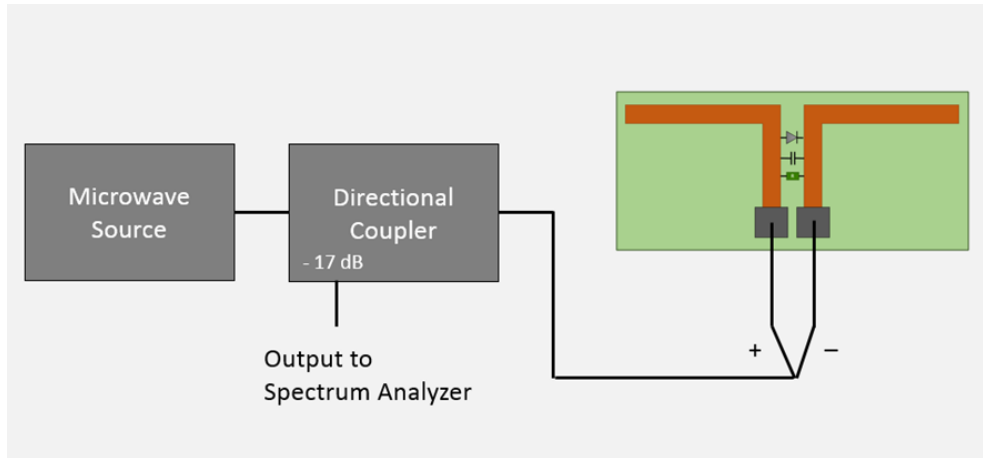


Figure 11-6: Experimental setup for harmonic generation testing.

## 11.5 Discussion

The intent of the rectenna was twofold. The rectenna was designed to rectify RF signals (1–10 GHz) and generate higher-order harmonics. Both of these qualities are needed for the creation of an NLTR rectifier. The current experiments establish a baseline for rectification and harmonic generation that can be used for future designs.

The current design has made no steps towards the impedance matching of the

antenna to the components. This is likely a major source of power lost by the system for rectification, and should be a top priority to consider in subsequent designs.

Our design of a dual-purpose rectenna satisfied our initial goals, and is a first step towards a functioning NLTR based WPT system. After considerable optimization and miniaturization, the rectenna would be used as a receiver for the electronics we want to power. After receiving the initial interrogation pulse and generating the 2nd harmonic response, it would then receive the main high power pulse and rectify the signal, providing the load device with DC power. Due to the nature of NLTR, the receiving devices don't require power to facilitate the process.



# Chapter 12

## Conclusion

### 12.1 Future Work

TODO:**This is RICK!**

### 12.2 Summary

TODO:...



## Appendix A

## Appendix A



## Appendix B

## Appendix B







# Bibliography

- [1] First GSM-based communicator product hits the market Nokia Starts Sales of the Nokia 9000 Communicator, August 1996.
- [2] A brief history of Wi-Fi. *The Economist*, June 2004.
- [3] APD Semiconductor. *AN-1012: Reverse Recovery Time (TRR) of the Super Barrier Rectifier*, 2006.
- [4] E. Barbieri and M. Meo. Time reversal DORT method applied to nonlinear elastic wave scattering. *Wave Motion*, 47(7):452–467, November 2010.
- [5] Kenneth Butler. Tour WiTricityâŽs Room of Tomorrow: Wireless Charging ThatâŽs Flexible, December 2013.
- [6] D. H. Chambers. Target characterization using time-reversal symmetry of wave propagation. *International Journal of Modern Physics B*, 21(20):3511–3555, August 2007.
- [7] Sam Davis. Schottky diodes: the old ones are good, the new ones are better. *Power Electronics*, 2011.
- [8] Matthew Frazier, Biniyam Taddese, Thomas Antonsen, and Steven M Anlage. Nonlinear time reversal in a wave chaotic system. *Physical review letters*, 110(6):063902, 2013.
- [9] Matthew Frazier, Biniyam Taddese, Bo Xiao, Thomas Antonsen, Edward Ott, and Steven M Anlage. Nonlinear time reversal of classical waves: Experiment and model. *Physical Review E*, 88(6):062910, 2013.
- [10] Eric Giler. A demo of Wireless Electricity, July 2009.
- [11] Dennis H Goldstein and Edward Collett. *Polarized light*. Marcel Dekker, New York, 2003.
- [12] Griffiths, David. *Introduction to Electrodynamics*. Prentice Hall, 3 edition, 1999.
- [13] Sameer Hemmady, Xing Zheng, James Hart, Thomas M Antonsen Jr, Edward Ott, and Steven M Anlage. Universal properties of two-port scattering, impedance, and admittance matrices of wave-chaotic systems. *Physical Review E*, 74(3):036213, 2006.

- [14] Sun K. Hong, Victor M. Mendez, Trystan Koch, Walter S. Wall, and Steven M. Anlage. Nonlinear Electromagnetic Time Reversal in an Open Semireverberant System. *Physical Review Applied*, 2(4), October 2014.
- [15] Morris Kesler. Highly Resonant Wireless Power Transfer: Safe Efficient and over Distance. Technical report, WiTricity, Watertown MA, 2013.
- [16] Keysight Technologies. *Infinium 90000 Series Oscilloscopes*. Rev. V8.
- [17] Macom. *GaAs Flip Chip Schottky Barrier Diodes*. Rev. V8.
- [18] Dinh-Quy Nguyen and Woon-Seng Gan. The DORT solution in acoustic inverse scattering problem of a small elastic scatterer. *Ultrasonics*, 50(8):829–840, August 2010.
- [19] C. Prada. The iterative time reversal mirror: A solution to self-focusing in the pulse echo mode. *The Journal of the Acoustical Society of America*, 90(2):1119, 1991.
- [20] Claire Prada, SÃ©bastien Manneville, Dimitri Spoliansky, and Mathias Fink. Decomposition of the time reversal operator: Detection and selective focusing on two scatterers. *The Journal of the Acoustical Society of America*, 99:2067, 1996.
- [21] John B Schneider. Understanding the finite-difference time-domain method. *School of electrical engineering and computer science Washington State University.–URL:* , 2010.
- [22] David Hope Simpson, Chien Ting Chin, and Peter N. Burns. Pulse inversion Doppler: a new method for detecting nonlinear echoes from microbubble contrast agents. *Ultrasonics, Ferroelectrics, and Frequency Control, IEEE Transactions on*, 46(2):372–382, 1999.
- [23] Walter Fox Smith. *Waves and oscillations: a prelude to quantum mechanics*. Oxford University Press, New York, 2010.
- [24] Young-Ho Suh and Kai Chang. A high-efficiency dual-frequency rectenna for 2.45-and 5.8-ghz wireless power transmission. *Microwave Theory and Techniques, IEEE Transactions on*, 50(7):1784–1789, 2002.
- [25] Binyam Tesfaye Taddese, Thomas M. Antonsen, Edward Ott, and Steven M. Anlage. Sensing small changes in a wave chaotic scattering system. *Journal of Applied Physics*, 108(11):114911, 2010.
- [26] Computer Simulation Technology. The finite integration technique. Retrieved from the CST website <https://www.cst.com/Products/CSTMws/FIT>.

- [27] N. Tesla. Apparatus for transmitting electrical energy. U.S. Patent, dec 1914. Patent US 1119732 A.
- [28] C.A. Tucker, K. Warwick, and W. Holderbaum. A contribution to the wireless transmission of power. *International Journal of Electrical Power & Energy Systems*, 47:235–242, May 2013.
- [29] M Clemens T Weiland. Discrete electromagnetism with the finite integration technique. *Progress In Electromagnetics Research*, 32:65–87, 2001.
- [30] Huiqing Zhai, Helen K. Pan, and Mingyu Lu. A practical wireless charging system based on ultra-wideband retro-reflective beamforming. In *Antennas and Propagation Society International Symposium (APSURSI), 2010 IEEE*, pages 1–4, 2010.